Remote Sensing of Environment 246 (2020) 111830

Contents lists available at ScienceDirect

Remote Sensing of Environment

journal homepage: www.elsevier.com/locate/rse

Machine learning estimators for the quantity and quality of grass swards used for silage production using drone-based imaging spectrometry and photogrammetry

Raquel Alves Oliveira[a,*], Roope Näsi[a], Oiva Niemeläinen[b], Laura Nyholm[c], Katja Alhonoja[d], Jere Kaivosoja[b], Lauri Jauhiainen[b], Niko Viljanen[a], Somayeh Nezami[a], Lauri Markelin[a], Teemu Hakala[a], Eija Honkavaara[a]

[a] Department of Remote Sensing and Photogrammetry, Finnish Geospatial Research Institute in National Land Survey of Finland (FGI), Finland
[b] Natural Resources Institute Finland (Luke), Finland
[c] Valio Ltd, Farm Services, Helsinki, Finland
[d] Yara Kotkaniemi Research Station, Yara Suomi Oy, Finland

ARTICLE INFO

Edited by Marie Weiss

Keywords:
Hyperspectral
Drone
Photogrammetry
Precise agriculture
Grass sward
Biomass
Digestibility
Nitrogen
Neutral detergent fibre
Machine learning
Random forest
Multiple linear regression

ABSTRACT

Drones offer entirely new prospects for precision agriculture. This study investigates the utilisation of drone remote sensing for managing and monitoring silage grass swards. In northern countries, grass swards are fertilised and harvested three times per season when aiming to maximise the yield. Information about the grass quantity and quality is necessary to optimise these operations. Our objectives were to investigate and develop machine-learning techniques for estimating these parameters using drone photogrammetry and spectral imaging. Trial sites were established in southern Finland for the primary growth and regrowth of grass in the summer of 2017. Remote-sensing datasets were captured four times during the primary growth season and three times during the regrowth period. Reference measurements included fresh and dry biomass and several quality parameters, such as the digestibility of organic matter in dry matter (the D-value), neutral detergent fibre (NDF), indigestible neutral detergent fibre (iNDF), water-soluble carbohydrates (WSC), the nitrogen concentration (Ncont) in dry matter (DM) and nitrogen uptake (NU). Machine-learning estimators based on random forest (RF) and multiple linear regression (MLR) methods were trained using the reference measurements and tested using independent test datasets. The best results for the biomass estimation, nitrogen amount and digestibility were obtained when using hyperspectral and 3D data, followed by the combination of multispectral and 3D data. During the training process, the best normalised root-mean-square errors (RMSE%) were 14.66% for the dry biomass and 12% for fresh biomass; the best RMSE% values for NU, the D-value and NDF were 13.6%, 1.98% and 3% respectively. For the primary growth, the accuracies of all quality parameters were better than 20% with the independent test datasets; for the regrowth, the estimation accuracies of the D-value, iNDF, NDF, Ncont and NU were better than 20%. The results showed that drone remote sensing was an excellent tool for the efficient and accurate management of silage production.

1. Introduction

Timely information about the properties of crops is required in order to facilitate the utilisation of precision agriculture technologies for sustainable agricultural production. By choosing suitable seed mixtures, fertiliser application rates and the timing of the harvest, grassland management aims to secure adequate yields of a desired quality for feeding at minimum cost and under the prevailing weather and edaphic conditions of production. In the Nordic countries, silage grass swards are harvested two to four times a season, and fertiliser is

* Corresponding author at: National Land Survey of Finland, Finnish Geospatial Research Institute FGI, Department of Remote Sensing and Photogrammetry, P.O. Box 84, FI-00521 Helsinki, Finland.

E-mail addresses: raquel.alvesdeoliveira@nls.fi (R.A. Oliveira), roope.nasi@nls.fi (R. Näsi), oiva.niemelainen@luke.fi (O. Niemeläinen), laura.nyholm@valio.fi (L. Nyholm), katja.alhonoja@gasum.com (K. Alhonoja), jere.kaivosoja@luke.fi (J. Kaivosoja), lauri.jauhiainen@luke.fi (L. Jauhiainen), niko.viljanen@nls.fi (N. Viljanen), snezami89@gmail.com (S. Nezami), lauri.markelin@nls.fi (L. Markelin), teemu.hakala@nls.fi (T. Hakala), eija.honkavaara@nls.fi (E. Honkavaara).

https://doi.org/10.1016/j.rse.2020.111830
Received 21 December 2018; Received in revised form 27 December 2019; Accepted 13 April 2020
Available online 11 May 2020
0034-4257/ © 2020 The Authors. Published by Elsevier Inc. This is an open access article under the CC BY license (http://creativecommons.org/licenses/BY/4.0/).

applied once for each harvest. Thus, information on the grass quantity and quality, provided several times in a growing season, is of high value for making decisions about the harvesting time and fertiliser application rate.

The fundamental quantity measures of swards are the fresh and dry biomass, which have well-described measurement methods in the sward research literature (e.g. Hopkins, 2000; 't Mannetje, 2000). The term 'fresh yield production' refers to the mass of herbage that can be removed by mechanical harvesting. Herbage production is expressed on an area basis for a given period, for example, the weight of dry matter (DM) kg/ha per cut or year. The small-plot cutting method is the most widely used technique for assessing herbage production in research studies (Hopkins, 2000). The basic operation involves cutting and weighing a sample of fresh herbage from a precisely measured area at a specified cutting height. After weighing, the sample is dried in an oven to determine the DM percentage, enabling the DM yield per unit area to be calculated (Hopkins, 2000). Indirect methods are used, particularly for grazing management purposes, and are usually manually measured from a few sample points in the field, using devices such as a rising plate meter, capacitance meter or meter stick ('t Mannetje, 2000; Sanderson et al., 2001; Virkajärvi, 1999). The ultimate quality assessment of the forage is carried out in feeding trials involving milk- or meat-production ruminants. Although this is an expensive method and requires a lot of feeding material, the method is continuously needed, for instance, in diet formulation studies (Rinne, 2000; Kuoppala, 2010). In vivo and in vitro methods have been developed and used to predict the digestibility of organic matter, which provides a measure of the available energy in the forage dry matter for the specified animal species (Rymer, 2000). Huhtanen et al. (2006) stated that the in vitro pepsin-cellulose solubility of organic matter and the concentration of indigestible neutral detergent fibre (iNDF) predicted the digestibility of organic forage matter with an acceptable accuracy for practical feed evaluation purposes. However, these methods are time consuming and laborious. Since Norris et al. (1976) introduced the near-infrared spectroscopy (NIRS) equations for forage quality laboratory estimation, the method has developed into a rapid and practical method and is used, for example, to follow the quality development of growing swards, as well as in silage quality analysis. Once the analyser is calibrated, the NIRS method is cheaper than the classical reference methods and studies have shown that there is a good agreement between the laboratory NIRS technique and the conventional methods (Aastveit and Marum, 1989). The NIRS analyses of commercial services make predictions for a large number of quality characteristics which are important for farmers. In Finland, the Valio dairy company provides NIRS predictions, for example, predictions of the digestibility of organic matter in dry matter (the D-value), neutral detergent fibre (NDF), iNDF, crude protein and water-soluble carbohydrate (WSC) values of forage for their contract farmers (http://valma.valio.fi/palvelut/).

In the Nordic countries' conditions, the feed quality of grass swards changes rapidly in the primary growth, when the proportion of stems in the yield increases (Nissinen et al., 2010). The OMD is reduced by more than one percentage unit per day during the fastest development period in the primary growth phase and the dry matter yield (DMY) increases by 220–240 kg/ha/day (Nissinen et al., 2010). In the work of Rinne (2000), the reduction of one percentage unit in the typical silage D-value decreased the energy-corrected milk production of cows by 0.50 kg/day and, consequently, the profitability of the farm. In this context, the timing of the harvest in the primary growth phase is very important (Rinne, 2000; Kuoppala, 2010). Information about the variation of the D-value within and among fields can simplify the management of the grass swards after harvesting, separating the forage by quality levels into respective silos, which can facilitate the optimal use of silage in feeding. In addition to feeding purposes, the nitrogen concentration (Ncont) in the yield is also an important parameter for sward management as, together with information on the DMY, it indicates how much of the applied fertiliser nitrogen was taken up by the sward. Thereby, the Ncont helps to determine the fertiliser application rate for the next harvest. Site-specific data on the yield, Ncont and nitrogen uptake (NU) can provide information on the nitrogen availability from soil and of the organic fertilisers for the sward.

Portable or field spectroradiometers (hyperspectral sensors) have also been used to estimate forage quantity and quality parameters, showing significant correlations between spectra and in situ vegetation (Hensen and Schjoerring, 2003; Pullanagari et al., 2012). Zheng and Chen (2018) investigated three stages of growth in a field with grass and alfalfa using measurements from a spectrometer to estimate biomass yield, NDF, acid detergent fibre and crude protein (CP). However, laboratory-based NIRS approaches, manual height measurements and hand-held spectrometers are not practical techniques for large areas or for providing complete spatial coverage of a field. Alternatively, several studies have shown the potential of using remote-sensing techniques to estimate crop parameters (Mulla, 2013; Higgins et al., 2017). Recently, drones (also referred to as *unmanned aircraft systems* and *remotely piloted aircraft systems*) have emerged as an effective, fast and low-cost platform for collecting remote-sensing data in agricultural applications (Bendig et al., 2014; Li et al., 2016; Näsi et al., 2018). In the last two decades, photogrammetric methods for dense 3D reconstruction based on aerial or terrestrial images have greatly advanced due to the development of computational technology and improvements in photogrammetric and computer-vision algorithms (Wu, 2013). These methods have been successfully applied in agriculture, for example, drones have been used to estimate biomass and detect individual plants.

Agricultural crop parameters have been estimated in various studies using multispectral imagery data (Berni et al., 2009; Candiago et al., 2015; Geipel et al., 2016) or hyperspectral imagery data (Capolupo et al., 2015; Zarco-Tejada et al., 2013; Näsi et al., 2018). The combination of 3D features based on photogrammetry or laser scanning and spectral image features has improved the estimation accuracy in several studies, especially for the biomass estimation of barley (Bendig et al., 2015; Näsi et al., 2018), winter wheat (Yue et al., 2017) and grass swards (Viljanen et al., 2018).

Past research on the use of remote-sensing image data in agriculture has mostly focused on biomass estimation (e.g. Bendig et al., 2014; Candiago et al., 2015; Yue et al., 2017; Viljanen et al., 2018) and only a few studies have explored quality parameters (Ali et al., 2016; Knoblauch et al., 2017; Pullanagari et al., 2018) other than focusing on nitrogen estimation (Li et al., 2016; Näsi et al., 2018). However, the management of silage grass swards especially requires knowledge about quality parameters in order to define the optimal harvesting time and overall management of the production.

The objective of this work was to develop and assess a machine-learning technique for the estimation of the quantity and quality of grass swards based on drone spectral imaging and photogrammetry. The contributions of this work are (i) the use of spectral and 3D features in quantity and quality grass crop parameter estimations, (ii) the comparison of RGB, multispectral and hyperspectral imaging–based remote sensing techniques, (iii) the assessment of the estimated prediction models from training data in order to estimate crop parameters in an independent test site and (iv) the estimation and evaluation of methods for different harvests and growths (primary growth and regrowth).

2. Materials and methods

2.1. Study area

Data from four experimental grass sites of a research farm owned by the Natural Resources Institute Finland (Luke) were used in this study. The study sites were located in the municipality of Jokioinen in southwest Finland (approximately 60° 48′ N, 23° 30′ E). One site was located in the Ilmala area of Jokioinen and it was used for training estimation models at the primary growth stage (PG_TR). The other

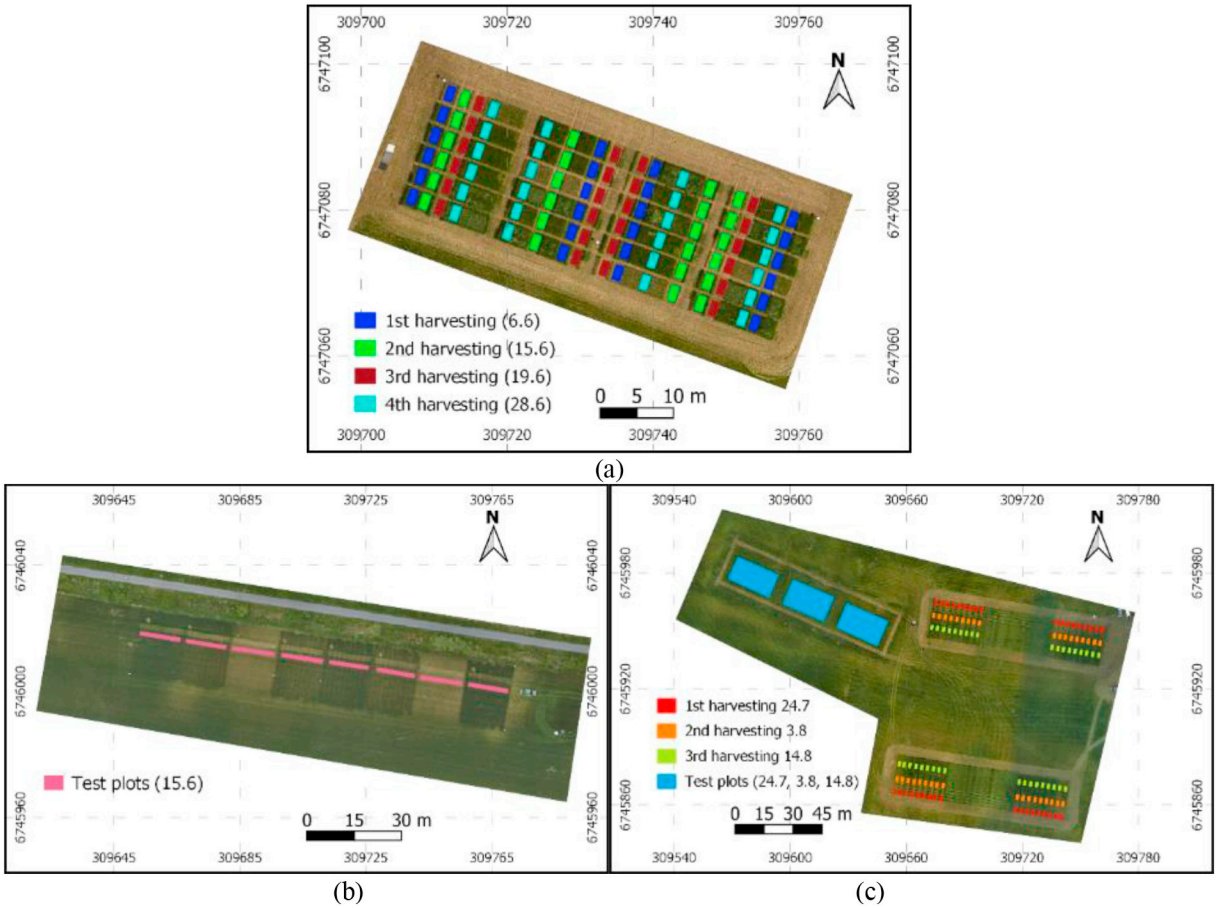

Fig. 1. An RGB orthomosaic and the location of harvesting dates for (a) the primary growth training area (PR_TR) (the orthomosaic is from a flight on the 28th of June), (b) the primary growth testing area (PR_TE) and (c) the regrowth study area and plots used as training and testing data (RG_TR, RG_TE).

three sites were in the Pellilä area of Jokioinen. In Pellilä, one site was used as testing data for the primary growth (PG_TE) models. The two remaining sites, which were located in different areas of the same field, were used for the training and testing of the regrowth stage (RG_TR and RG_TE, for the training and testing respectively).

The sward data PG_TR (Fig. 1a) was for a second-year timothy meadow fescue (*Phleum pratense* and *Festuca pratensis*) crop, which was managed as a silage production sward in 2016. The soil type was clay. In spring 2017, a uniform part of the field was selected for the agriculture experiments and was divided into plots for the application of different fertiliser rates. Fertiliser treatment was applied on the main plot (plot size: 12 m × 3 m), and the harvest was taken from the subplot on different dates. The experiment had a total of 96 plots (Fig. 1a), which consisted of four replicates, six nitrogen fertiliser levels (0, 50, 75, 100, 125 and 150 kg ha^{-1}) and four harvesting/measuring dates (the 6th, 15th, 19th and 28th of June). The fertiliser application was carried out on the 10th of May 2017 using an experimental surface fertiliser spreader with a working width of 1.5 m (a tailor-made model), manufactured at Luke. The manually moved spreader was designed to provide accurate amounts of granulated fertiliser on the soil surface. From each of the 96 plots, 2.6 m long samples were harvested using a Haldrup forage plot harvester with 1.5 m cutting bar. In the primary growth experiments, drone-based RGB and hyperspectral datasets were collected on the same days as each harvest. More details of the PG_TR data are presented by Viljanen et al. (2018).

The experimental grass field used for testing the primary growth estimation models (PG_TE) was located approximately 1.2 km from the PG_TR test site (Fig. 1b). The soil of the field was clay with 7.3% organic matter. The sward was a second-year sward, established on the 2nd of June in 2015 with a seed mixture composing of 67% timothy fescue and 33% tall fescue. However, the stand composition was nearly pure timothy in 2017. Test plots sized 15 m by 22 m were treated with four different nitrogen fertiliser rates (0, 50, 100 and 150 kg N ha^{-1}) with two replicates for each. The whole trial was set up in a 120 m long and 22 m wide rectangle (Fig. 1b). The spring nitrogen fertiliser was applied on the 11th of May 2017. The test sward was harvested using the same harvester and on the same dates as those for the training site, but the harvested plot length ranged from 12.65 m to 13.4 m.

The experiments for the training and the testing sites for the regrowth were established in the same field that was used for the testing data for the primary growth (Fig. 1c). For the regrowth experiments, the field was first fertilised for primary growth on the 5th of May 2017 (spring) using NPKS fertiliser (20-2-12-3) at a rate of 500 kg ha^{-1}, which provided 100 kg N ha^{-1} and was then harvested for silage on the 19th of June 2017. The fertiliser applications for the regrowth experiment were carried out on the 22nd of June 2017. The nitrogen application rates were 0, 25, 50, 75, 100, 125 and 150 kg N ha^{-1}. In addition to these seven nitrogen fertiliser application rates, two alternative nitrogen-source (ammonium sulphate and organic liquid nitrogen fertiliser) treatments, aiming to deliver 100 kg N ha^{-1}, were carried out. The plot size in this trial was 2.5 m by 20 m (Fig. 1c). On the two first harvesting dates (the 25th of July and 1st of August), around 3 m long samples of the plots were harvested each time using a Haldrup forage plot harvester. On the third harvest date (the 15th of August), an approximately 10 m long sample was harvested. After the three harvest dates, a total of 108 samples were collected. Drone flights were carried out on the same day as the harvest, or one day before the harvest, except for the cut on the 1st of August when the flight was carried out two

Table 1
Reference measurements for primary growth. Min: minimum; max: maximum; mean: average; std: the standard deviation of the attribute; FY: fresh yield; DMY: dry matter yield; D-value: digestible organic matter in dry matter; iNDF: indigestible neutral detergent fibre; NDF: neutral detergent fibre; WSC: water-soluble carbohydrates; Ncont: nitrogen concentration; NU: nitrogen uptake. PR_TR: primary growth training area; PR_TE: primary growth testing area (PR_TE).

		FY (kg/ha)	DMY (kg DM/ha)	D-value (g/kg DM)	iNDF (g/kg DM)	NDF (g/kg DM)	WSC (g/kg DM)	Ncont (g N/kg DM)	NU (N kg/ha)
PG_TR 6 June	Min	1022	336	734	27	435	104	22.56	7.79
	Max	5975	1703	770	52	464	225	40.80	62.42
	Mean	3921	1113	754	38	446	153	32.45	37.83
	Std	1488	360	12	8	9	38	5.63	16.32
PG_TR 15 June	Min	2133	625	719	11	528	80	16.48	10.30
	Max	17,143	3329	764	40	591	209	28.32	85.02
	Mean	10,592	2258	734	30	566	126	22.26	52.62
	Std	4268	746	13	6	17	40	3.85	22.84
PG_TR 19 June	Min	1716	531	652	50	522	76	14.40	7.64
	Max	21,138	4349	724	104	614	203	25.92	100.18
	Mean	12,691	2906	693	78	566	120	18.61	56.59
	Std	5720	1168	18	13	23	38	2.86	27.50
PG_TR 28 June	Min	2614	856	632	81	515	99	11.84	10.41
	Max	25,459	6135	695	128	599	246	19.52	105.69
	Mean	16,979	4333	660	103	573	156	14.93	67.36
	Std	7343	1611	18	13	22	42	2.35	30.58
PG_TE 15 June	Min	4796	1256	708	29	573	79	16	21.10
	Max	18,783	3822	741	49	605	160	27.84	103.97
	Mean	11,206	2408	721	41	591	108	21.66	54.39
	Std	4440	816	12	6	11	31	4.33	25.97

days after the harvest (the 3rd of August) using the remaining part of the plot that corresponded to the harvested area.

For the regrowth testing data (RE_TE), three 30 m by 20 m plots (Fig. 1c) were fertilised on the 22nd of June with 25, 75 or 125 kg N ha^{-1} after the first cut (on the 19th of June 2017). For each harvest date (on the 26th of July, the 1st of August and the 15th of August 2017), one sample from each plot was harvested using a Haldrup forage plot harvester. The length of the harvested area ranged from 2.7 m to 3.75 m and the working width of the harvested area was 1.5 m. A representative sample (around 1 kg in fresh weight) was taken from each plot harvest for the quantity and quality analyses. From the nine independent test samples collected, we removed one sample from the last harvest date with the highest nitrogen application since the sample characteristics were out of the training data range; therefore, eight independent test samples were available.

2.2. Reference field data

The idea of the experimental set up was to generate variation in the study sward. General guidelines advise an application rate of 100 kg ha^{-1} for silage production in clay soil and a target D-value of 690 g/kg DM in the first harvest, which usually occurs close to the heading of grass species.

The development of primary growth grass swards in Finland depends on the accumulated temperature sum. The start of the growing season in Jokioinen was late in 2017 (on the 5th of May) and the early summer was cool. In 2017, the targeted D-value was reached around the 19th of June in Jokioinen. Therefore the harvest and observation dates on the 15th and 19th of June 2017 were around the optimum harvest time. The first harvest on the 6th of June was at a very early developmental stage of the sward, and on the 28th of June, the optimum harvest period had passed.

The zero-nitrogen application sward was sparse and weak, particularly on the first observation dates for both the primary growth and the regrowth. The highest nitrogen application rates – 125 and 150 kg N ha^{-1} at the PG_TR site, and 100, 125 and 150 kg N ha^{-1} in Pellilä (PG_TE, and RG_TR and RG_TE) – produced a dense sward which was susceptible to lodging, and this affected the growth of the stand prior to the last harvesting dates in both the primary growth and the regrowth. In addition, the highest nitrogen application rates seemed to increase the share of meadow fescue in the sward on the latest harvesting dates at the PG_TR site. Otherwise, the swards predominantly consisted of timothy. The training data for the regrowth was obtained from a 'NESTERAVINNE' project experiment in which the effect of the delayed application of slurry (liquefied animal manure) on sward growth and quality was the main research topic. This resulted in a longer than normal period from the harvest of the primary growth (on the 19th of June) to the harvest of the regrowth. In our study, the period was at five, six and eight weeks, with the three harvest dates of the 25th of July, and the 1st and 15th of August 2017, while the normal period is from four to six weeks. The weather conditions remained cool and rainy during the regrowth period, and the fresh yields (FYs) and DMYs obtained in the regrowth were high in this trial, as well as in general in Finland in 2017.

Reference measurements included the FY, DMY and feeding quality analysis. The samples collected from each harvested plot were weighed to determine FY and were then chopped into 3–4 cm long pieces by a Wintersteiger sample chopper (Model Hege 44), and the DMY was determined after overnight drying at 105 °C in forced-air drying ovens (a Memmert or Heraus). A similar sample for quality analyses was dried at 60 °C until dry. The feed quality analyses included predictions for the Ncont, NDF, iNDF, the D-value and WSCs and they were carried out by the Valio Ltd feed laboratory using the NIRS technique with Foss NIR XDS equipment. The D-value parameter is directly related to metabolised energy (ME) as a D-value (g/kg DM) multiplied by 0.016 provides ME as MJ/kg DM. Ncont is related to CP as Ncont (g N/kg DM) multiplied by 6.25 gives the CP value (g/kg DM). The resulting field measurements are presented in Tables 1 and 2.

The calibration set of the Valio Ltd NIRS analyser covers a wide range of variation in all the quality parameters involved in this study, which is necessary as we generated great variability in the test material by using different nitrogen application rates and harvest times. The NU by sward was calculated from both the Ncont in the DMY and the amount of DMY.

The Finnish Feed Tables service (https://portal.mtt.fi/portal/page/portal/Rehutaulukot/feed_tables_english) provides guideline values of

Table 2
Reference measurements for regrowth. Min: minimum; max: maximum; mean: average; std.: standard deviation of the attribute; FY: fresh yield; DMY: dry matter yield; D-value: digestible organic matter in dry matter; iNDF: indigestible neutral detergent fibre; NDF: neutral detergent fibre; WSC: water-soluble carbohydrates; Ncont: nitrogen concentration; NU: nitrogen uptake. RG_TR: regrowth training area; and RG_TE: regrowth testing area.

		FY(kg/ha)	DMY (kg DM/ha)	D-value (g/kg DM)	iNDF (g/kg DM)	NDF (g/kg DM)	WSC (g/kg DM)	Ncont (g N/kg DM)	NU (N kg/ha)
RG_TR 25 July	Min	1379	368	670	13	442	50	17.92	7.54
	Max	24,598	3860	756	82	573	242	33.12	124.12
	Mean	13,685	2546	717	44	533	117	24.10	64.37
	Std	6664	1017	21	19	37	61	4.23	32.82
RG_TR 1 August	Min	2000	606	668	15	426	61	15.84	11.87
	Max	26,909	4696	748	89	612	275	28.80	129.99
	Mean	16,067	3339	697	55	547	129	20.76	71.94
	Std	7056	1232	24	21	47	65	3.48	33.22
RG_TR 15 August	Min	2810	917	618	53	440	89	12.96	12.77
	Max	32,391	7229	718	137	609	294	20.96	132.94
	Mean	20,223	4744	655	99	558	166	15.58	75.16
	Std	9003	1683	24	18	46	58	2.18	30.78
RG_TE (25 July, 1 August, 15 August)	Min	7843	2073	631	57	464	89	14.08	37.83
	Max	36,135	8047	714	114	575	207	28.48	150.60
	Mean	19,254	4360	674	85	535	141	20.07	84.77
	Std	9284	2053	29	21	36	47	4.81	35.59

D-value and CP concentration for different harvesting time, in the primary growth and regrowth, considering the fertiliser application of 100 kg N ha^{-1} for grass swards cultivated according to recommended agricultural practice. The D-values obtained in the reference data in both the primary growth and in the regrowth covered the whole range presented in the Finnish Feed Tables well (see Tables 1 and 2). For nitrogen concentration, the range in the reference data was wider than in the guidelines, which was expected as the applied nitrogen fertiliser rate ranged from 0 to 150 kg N ha^{-1} while in practical farming this range varies from 75 to 100 kg N ha^{-1} for both the primary and regrowth stands.

The relation between biomass and digestibility can be seen in Fig. 2, which shows the primary growth and regrowth field measurements for the DMY and the D-value for the nitrogen fertilisation level N100. These are negatively correlated in the primary growth as usually, as the quantity increases, the quality – measured as a D-value – decreases, which occurred also for the regrowth in this study.

The Pearson correlation coefficients (PCCs) of the primary growth reference data parameters (Fig. 3) also show that the biomass parameters (FY, DMY) and the D-value were strongly negatively correlated.

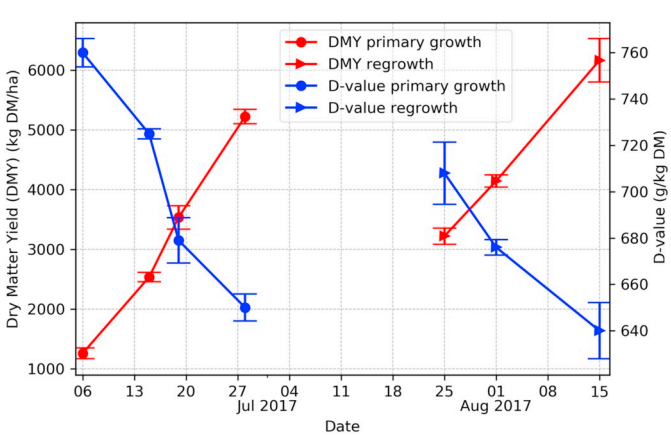

Fig. 2. The reference measurements for the primary growth and regrowth for the DMY (dry matter yield) and the D-value (organic matter in dry matter) for the nitrogen fertilisation level N100. Standard deviation is shown as an error bar.

The D-value attribute was also inversely correlated with the iNDF (PCC: −0.95). The negative correlation of the D-value with the FY and DMY, as well as the iNDF, is the major issue to be monitored in order to achieve a balance between an adequate yield and adequate quality (see e.g. Rinne, 2000; Nissinen et al., 2010). In the regrowth measurements, the correlations between most of the attributes were comparable to the primary growth, but Ncont presented smaller correlation between biomass, D-value, iNDF and NDF and higher correlation with WSC and NU.

2.3. Remote-sensing data sets

The acquisition of remote-sensing datasets was carried out using a drone assembled by the Finnish Geospatial Research Institute (FGI). The FGI's drone has a Gryphon Dynamics quadcopter frame with detachable arms and it is equipped with a Pixhawk 1 autopilot flight control unit running Arducopter firmware. The drone has been designed to operate using different sensors and is able to fly for 25 min carrying a payload of 4 kg (Fig. 4).

The drone was equipped with an NV08C-CSM L1 single-frequency global navigation satellite system (GNSS) receiver (NVS Navigation Technologies Ltd., Montlingen, Switzerland), a Raspberry Pi single-board computer (Raspberry Pi Foundation, Cambridge, United Kingdom), a 36.4 megapixel Sony A7R (RGB) camera (Sony Corporation, Minato, Tokyo, Japan) with a Sony FE 35 mm f/2.8 ZA Carl Zeiss Sonnar T* lens (Sony Corporation, Minato, Tokyo, Japan) and a hyperspectral 2D frame camera (the prototype FPI2012b) based on a Fabry-Pérot interferometer (FPI) adjustable filter, which acquires spectral bands using a time sequence–based process (i.e. the acquisition is not simultaneous for all bands of the same hyperspectral cube) (Oliveira et al., 2016; Honkavaara et al., 2017). The FPI camera system weighs < 700 g. The image size is 1024 × 648 pixels with a pixel size of 11 μm and the nominal focal length is 10.9 mm (Mäkynen et al., 2011; Honkavaara et al., 2013). The prototype FPI2012b was configured to capture hyperspectral images on 36 bands in the range of 500–900 nm (Table 3).

The RGB and the hyperspectral cameras were triggered to capture images at two-second intervals. The PPS (pulse-per-second) signal from the GNSS unit and synchronisation pulses were recorded for each exposure of each camera (i.e. for each band of the hyperspectral camera) using the Raspberry Pi 3 GPIO. The PPS signal was used to calibrate the

	FY	DMY	D-value	iNDF	NDF	WSC	Ncont	NU
FY	*	0.97	-0.80	0.68	0.78	-0.60	-0.35	0.92
DMY	0.97	*	-0.85	0.77	0.74	-0.48	-0.41	0.87
D-value	-0.80	-0.85	*	-0.95	-0.73	0.20	0.65	-0.59
iNDF	0.68	0.77	-0.95	*	0.54	-0.08	-0.58	0.49
NDF	0.78	0.74	-0.73	0.54	*	-0.42	-0.68	0.57
WSC	-0.60	-0.48	0.20	-0.08	-0.42	*	-0.34	-0.79
Ncont	-0.35	-0.41	0.65	-0.58	-0.68	-0.34	*	0.03
NU	0.92	0.87	-0.59	0.49	0.57	-0.79	0.03	*

Fig. 3. The correlations for the reference data of the primary growth measurements. FY: fresh yield; DMY: dry matter yield; D-value: digestible organic matter in dry matter; iNDF: indigestible neutral detergent fibre; NDF: neutral detergent fibre; WSC: water-soluble carbohydrate; Ncont: nitrogen concentration; NU: nitrogen uptake.

timestamps to GPS time at a microsecond resolution. Afterwards, the data from the GNSS positions for each camera were computed using post-processed kinematic (PPK) in RTKLIB software (RTKLIB version 2.4.2, open source, Raleigh, NC, USA) (RTKLIB, 2018). Observation data from the FinnRef stations of the National Land Survey of Finland (NLS) RINEX service (NLS, 2018) was used in the PPK processing.

Table 4 presents the flight parameters and weather conditions of the remote-sensing datasets captured during the primary growth, throughout June of 2017, and during the regrowth, from the end of July to the middle of August in 2017.

The flight heights of the campaigns in Jokioinen were 50 m, except for one flight (PG_TR_20170615), giving a ground sampling distance (GSD) of 5 cm for the hyperspectral data and 0.64 cm for the RGB data. The flight PG_TR_20170615 was at a height of 30 m, thus the GSDs for the hyperspectral data and for the RGB data were 3 cm and 0.39 cm respectively. The flight speed was 2 m/s in all flights. Image overlaps were about 84–87% in the forward direction and 65–81% between flight lines.

2.4. Remote-sensing data processing

2.4.1. Geometric processing

The accurate geometric processing of image datasets is essential when combining data collected on different flights, dates and/or from different sources. A rigorous photogrammetric workflow was carried out for all datasets, aiming to determine the image exterior orientation parameters (EOPs), camera interior orientation parameters (IOPs), 3D point clouds and orthomosaics. The photogrammetric workflow was done using Agisoft PhotoScan Professional software (version 1.3.4, Agisoft LLC, St. Petersburg, Russia). The image alignment processes of each dataset were performed using a high quality setting, with 40,000 key points and 4000 tie points per image; 3D coordinates of each camera exposure – collected by the on-board GNSS receiver and approximate values of the camera IOPs (principal distance, principal point, and radial and tangential lens distortions) – were inserted in Agisoft PhotoScan as initial values for the alignment adjustment (self-calibration). For each test site, five ground control points (GCPs) were surveyed using a Trimble R10 RTK DGNSS with 0.03 m horizontal accuracy and 0.04 m vertical accuracy. These GCPs were manually measured in the images. We considered the a priori standard deviation to be ± 0.005 m for GCPs and ± 5 m for the image coordinates. After the initial alignment processing, tie point outliers were removed using

Table 3
The spectral settings of the hyperspectral frame camera prototype FPI2012b. L0: central wavelength; FWHM: full width at half maximum.

L0 (nm):	512.3, 514.8, 520.4, 527.5, 542.9, 550.6, 559.7, 569.9, 579.3, 587.9, 595.9, 604.6, 613.3, 625.1, 637.5, 649.6, 663.8, 676.9, 683.5, 698.0, 705.5, 711.4, 717.5, 723.8, 738.1, 744.9, 758.0, 771.5, 800.5, 813.4, 827.0, 840.7, 852.90, 865.3, 879.6, 886.5
FWHM (nm):	14.81, 17.89, 20.44, 21.53, 19.50, 20.66, 19.56, 22.17, 17.41, 17.56, 21.35, 20.24, 25.30, 27.63, 24.59, 27.86, 26.75, 27.00, 28.92, 24.26, 24.44, 25.12, 27.45, 27.81, 26.95, 25.56, 27.78, 27.61, 23.82, 28.28, 26.61, 26.85, 27.54, 28.29, 25.89, 23.69

Fig. 4. The drone and payload.

Table 4
Flight parameters for each dataset: date, time, weather, sun azimuth, solar elevation. FH: flight height; FL: number of flight lines; PR_TR: primary growth training area; PR_TE: primary growth testing area; RG_TR: regrowth training area; and RG_TE: regrowth testing area.

Dataset	Date	Time (GNSS)	Weather	Sun azimuth (°)	Solar elevation (°)	FH (m)
Training data – primary growth						
PG_TR_20170606	6 June	12:26 to 12:34	Varying	217.85	51.28	50
PG_TR_20170615	15 June	08:59 to 09:14	Sunny	150.21	49.96	30
PG_TR_20170619	19 June	09:09 to 09:26	Varying	153.34	50.58	50
PG_TR_20170628	28 June	07:13 to 07:29	Sunny	117.47	40.45	50
External testing data – primary growth						
PG_TE_20170615	15 June	13:22 to 13:35	Cloudy	241.13	48.91	50
Training and external testing data – regrowth						
RG_TR20170724/RG_TE20170724	24 July	08:55 to 09:18	Cloudy	151.24	43.51	50
RG_TR20170803/RG_TE20170803	3 August	09:59 to 10:22	Varying	174.06	43.50	50
RG_TR20170814/RG_TE20170814	14 August	11:43 to 12:06	Varying	214.54	50.53	50

automatic tools based on re-projection residuals and the standard deviations of the tie point 3D coordinates, and in some cases, outlier points were manually removed (see more details in the work of Nevalainen et al., 2017; Näsi et al., 2015).

The alignment step was done as described above for the RGB datasets, and for the RGB and three bands of the FPI hyperspectral images (RGBFPI; band 5: L0 = 542.9 nm; band 11: L0 = 595.9; band 14: L0 = 625.1 nm). The root-mean-square errors (RMSEs) of the residuals in the image coordinates (re-projection errors) estimated for the RGBFPI blocks were 0.35–0.74 pixels and the RMSEs of the differences at GCPs varied from 0.21 to 1.23 cm in horizontal and vertical directions (Table 5).

Once the RGB images were aligned, dense 3D point clouds were generated by PhotoScan using the 'High' and 'Mild' depth filtering settings. Next, the 3D point clouds were interpolated in order to generate digital surface models (DSMs) and orthomosaics. The outputs of the geometric processing were camera IOPs and EOPs, sparse point clouds (tie points), DSMs and RGB orthomosaics. The RGB orthomosaics were transformed from digital values (DNs) to reflectance values using the empirical line method (Smith and Milton, 1999) with three reflectance panels and an exponential function. Canopy height models (CHMs) were created from the photogrammetric DSMs of each dataset using the procedure described by Viljanen et al. (2018). We generated the digital terrain model (DTM) by classifying the ground points automatically using PhotoScan's 'classify ground points' tool. The parameters selected for all datasets were: a 3 m cell size, 0.5° for the maximum angle and a maximum distance of 2.0 cm. These parameters were selected based on visual inspection of the RGB orthomosaics. After the points were classified, ground points were interpolated, generating the DTMs of each area at a resolution of 1 cm. The DTMs and DSMs were exported as TIFF images and imported into the QGIS (version 2.18.14, Open-source, Raleigh, NC, USA) software to generate the CHMs by subtracting the DTM from the DSM.

The geometric processing in PhotoScan resulted in orientations for three reference bands of the FPI hyperspectral datasets. In order to generate orthomosaics for all bands, the EOPs of the remaining bands were estimated using the 3D band-matching approach developed by Honkavaara et al. (2017). From the three bands used in the geometric processing, the 542.9 nm and 800.5 nm bands were selected as reference bands for the 3D band matching; these bands are simultaneously acquired. The 542.9 nm band was utilised as a reference for the bands in the visual range and the 800.5 nm band was used for the bands in the NIR range. Additionally to the reference bands' EOPs and the camera's IOPs estimated in the geometric process, a sparse point cloud (tie points) with about 1000 points per image was also an input for the 3D band-matching procedure. The parameters in the 3D band-matching computation were selected based on the work of Honkavaara et al. (2017). The averages of the RMSEs of the image residuals after the band matching were 6.80–7.96 μm, indicating an accuracy better than one GSD of alignment, and were consistent with the results of Honkavaara et al. (2017).

2.4.2. Radiometric processing

The radiometric values of the same point can vary due to many physical issues at the moment of data acquisition, such as atmospheric effects, variable weather conditions and sensor non-uniformity. Furthermore, values are anisotropic as a function of the illumination and viewing direction, which can be modelled using the bidirectional reflectance distribution function (BRDF) (Schaepman-Strub et al., 2006). As a result, radiometric calibration and correction are crucial in order to obtain uniform and comparable imagery data for temporal analysis.

The radiometric processing of the hyperspectral images followed the approach proposed and developed by Honkavaara et al. (2013, 2018), which includes sensor corrections, atmospheric correction, correction for the radiometric non-uniformities caused by illumination variations,

Table 5
Bundle block adjustment dataset parameters: GSD: ground sampling distance; FPI: fabry-Perót interferometer hyperspectral camera, No: number of images; Rep. error: re-projection error; GCPs: ground control points; and RMSE: the root mean square error of X, Y and Z coordinates; PR_TR: primary growth training area; PR_TE: primary growth testing area; RG_TR: regrowth training area; and RG_TE: regrowth testing are.

Flight	No. of FPI cubes	No. of RGB images	Rep. error (pix)		GCPs RMSE RGB			GCPs RMSE RGBFPI		
			RGB	RGBFPI	X (cm)	Y (cm)	Z (cm)	X (cm)	Y (cm)	Z (cm)
PG_TR_20170606	111	156	0.78	0.57	0.64	0.41	1.47	0.79	0.80	0.97
PG_TR_20170615	158	174	0.59	0.36	0.28	0.38	0.75	0.27	0.27	0.33
PG_TR_20170619	226	320	1.12	0.48	0.58	1.31	0.27	0.56	1.15	0.22
PG_TR_20170628	211	350	1.25	0.51	0.32	0.52	1.61	0.26	0.47	0.21
PG_TE_20170615	158	197	0.33	0.37	0.81	1.18	0.51	0.83	1.23	0.55
PG_TR20170724/PG_TE20170724	291	555	0.76	0.66	0.61	0.79	1.52	0.49	0.69	1.23
PG_TR20170803/PG_TE20170803	316	591	0.89	0.74	0.90	0.92	0.51	0.85	0.83	0.48
PG_TR20170814/PG_TE20170814	316	519	0.69	0.66	0.27	1.22	0.22	0.33	1.18	0.35

Table 6
An overview of different features sets. The equations of vegetation indices are given by Viljanen et al. (2018) and Näsi et al. (2018).

Feature set labels	Description	N of features
RGB_3D	3D features based on canopy height models (CHMs) from RGB bands: mean height, minimum height, maximum height, standard deviation height, (50, 70, 80, 90th) percentile	8
RGB_b	Bands: Red, Green, Blue	3
RGB_i	Vegetation indices using RGB bands and CHMs: Green Red Vegetation Index (GRVI), Tucker (1979); Modified Green Red Vegetation Index (MGRVI), Bendig et al. (2014); Red Green Blue Vegetation Index (RGBVI), Bendig et al. (2015); Excess Green Index (ExG), Woebbecke et al. (1995); Excess Red Index (ExR), Meyer et al. (1999); Excess GreenRed Index (ExGR), Neto (2004); Grassland Index (GrassI), Bareth et al. (2015); Excess Green Combined with CHM (ExG + CHM), Viljanen et al. (2018);	8
MS_i	Vegetation indices using two spectral bands of hyperspectral camera: Normalised Difference Vegetation Index (NDVI), Rouse et al., 1974; Ratio Vegetation Index (RVI), Pearson and Miller (1972); Modified Soil-Adjusted Vegetation Index (MSAVI), Qi et al. (1994); Optimisation of Soil-Adjusted Vegetation Index (OSAVI), Rondeaux et al. (1996);	4
HS_b	The spectral bands of a hyperspectral camera (Table 3)	35
HS_i	Spectral indices based on a hyperspectral camera: NDVI, OSAVI, Ratio Difference Vegetation Index (RDVI), Roujean and Breon (1995); red-edge inflection point (REIP), Guyot and Baret (1988); Green Normalised Difference Vegetation Index (GNDVI), Gitelson et al. (1996); Modified Chlorophyll Absorption Ratio Index (MCARI), Daughtry et al. (2000); Modified Triangular Vegetation Index (MTVI), Haboudane et al. (2004); MERIS terrestrial chlorophyll index (MTCI), Dash and Curran (2004); Chlorophyll index green (Cl-red-edge), Gitelson et al. (2003); Chlorophyll index red-edge (Cl-green), Gitelson et al. (2003); Photochemical Reflectance Index (PRI[512.531]), Hernández-Clemente et al. (2011).	11

BRDF correction and absolute reflectance transformation. The sensor corrections included a photon response non-uniformity (PRNU) correction, done in the laboratory, and dark signal correction using an image obtained with the lens covered before the start of each flight. Both methods were performed using software produced by VTT (VTT Technical Research Centre of Finland Ltd) (Mäkynen et al., 2011). In-house radiometric block adjustment software, RadBA (Honkavaara et al., 2013; Honkavaara and Khoramshahi, 2018), was used for the other radiometric corrections and generation of the reflectance orthomosaics for each spectral band. The algorithm attempts to determine the radiometric model parameters by minimising the differences between the observed and modelled DNs of radiometric tie points in the overlapping images. For the radiometric modelling, the solar illumination geometry and, if available, irradiance information registered during the data acquisition are used. RadBA software can also integrate the DN multiple view observations of reflectance panels in the adjustment process for each band for the reflectance transformation. To enable the reflectance transformation, panels sized 1 m × 1 m, with the nominal reflectance of 0.03, 0.10 and 0.50, were positioned near the drone take off location. Images affected by cloud shadow were eliminated from the process. We used relative and BRDF corrections for the blocks captured under sunny conditions and only relative corrections for datasets captured in cloudy weather (Table 6). The processing provided uniform reflectance orthomosaics, as can be seen in Figs. 5, 6 and 7.

2.5. The extraction of features from the remote-sensing datasets

Spectral vegetation indices and 3D features were extracted from the hyperspectral and RGB mosaics and DSMs (Table 6). From the hyperspectral data, 35 bands were used to extract spectral features (HS_b). Additionally, the hyperspectral data were used to compute 11 spectral indices (HS_i). From the RGB data, three bands were used as features (RGB_b), in addition to eight spectral indices computed from the RGB bands and CHMs (RGB_i) and four multispectral vegetation indices (MS_i) calculated using two bands of the hyperspectral data. Table 6 lists the vegetation indices used. The 3D features were calculated using the CHMs generated from the RGB images (RGB_3D) for each dataset. A shapefile containing polygons of each plot's boundary, considering a margin of 0.25 m to avoid possible border effects, guided the feature-extraction process from the orthomosaics in the QGIS software (version 2.18.15, open source, Raleigh, NC, USA) using the 'zonal statistics' tool. The 3D features were obtained using a script implemented in Matlab software (version 2016b, MathWorks, Natick, MA, USA).

The correlations (PCCs) between each physical measurement and features extracted from the remote-sensing datasets of the primary growth (Fig. 8) and regrowth (Fig. 9) show that the quantity attributes FY and DMY were highly correlated with several extracted features, such as 3D features, multispectral-3D vegetation indices (PCCs from 0.76 to 0.91), RGB indices (RGBI, GRVI and ExG) (PCCs from 0.67 to 0.87), multispectral vegetation indices (PCCs from 0.71 to 0.91), hyperspectral green- to red-edge bands (PCCs from −0.72 to −0.81) and hyperspectral spectral NIR bands (bands 744.9 nm to 886.5 nm; PCCs from 0.72 to 0.89), and hyperspectral indices (PCCs from 0.69 to 0.89). Similar results were observed for the NU, iNDF and NDF. The D-value demonstrated similar PCCs to the FY and DMY but with inverse correlations (Fig. 8b). In the regrowth, the PCCs for the FY, DMY, iNDF, NDF and NU attributes decreased in the bands of the red-edge region in comparison with the primary growth. The WSC parameter presented smaller PCC values in the visible range but higher values of negative correlation in the NIR and hyperspectral indices while the D-value presented smaller correlations in the NIR range than in the primary growth. The Ncont parameter also had higher PCCs in the NIR bands and hyperspectral indices.

2.6. Estimation process and quality assessment

The estimation process used in this study is based on the methods proposed by Näsi et al. (2018) and Viljanen et al. (2018). Random forest (RF) and multiple linear regression (MLR) algorithms were used as estimators and the results were compared.

The RF is an ensemble learning technique introduced by Breiman (2001). The RF has been used in several remote-sensing fields because it can provide accurate predictions for classification, regression and several different machine-learning problems (Belgiu and Drăguţ, 2016). Studies have indicated that RF is insensitive to the presence of irrelevant predictors and that variable reduction does not impact significantly on the performance (Heung et al., 2014; Li et al., 2017). The RF's implementation in Weka software (Weka 3.8.1, University of Waikato) was used in the estimation phase of the grass parameters for feature selection and for validation. The number of decision trees was set to 500 and other parameters were set to their defaults.

MLR is a method that attempts to estimate the parameters of the model that describes the relationship between two or more independent variables and a response variable by fitting a linear equation to the observed data, often using the least squares method. We used the MLR implementation in Weka (Weka 3.8.1, University of Waikato). In Weka, the selection of the features model was done using a backward elimination method called 'M5', wherein the attribute with the smallest standardised coefficient is removed until no improvements are observed in the Akaike information criterion (Akaike, 1974).

Multiple feature combinations were formed based on RGB and

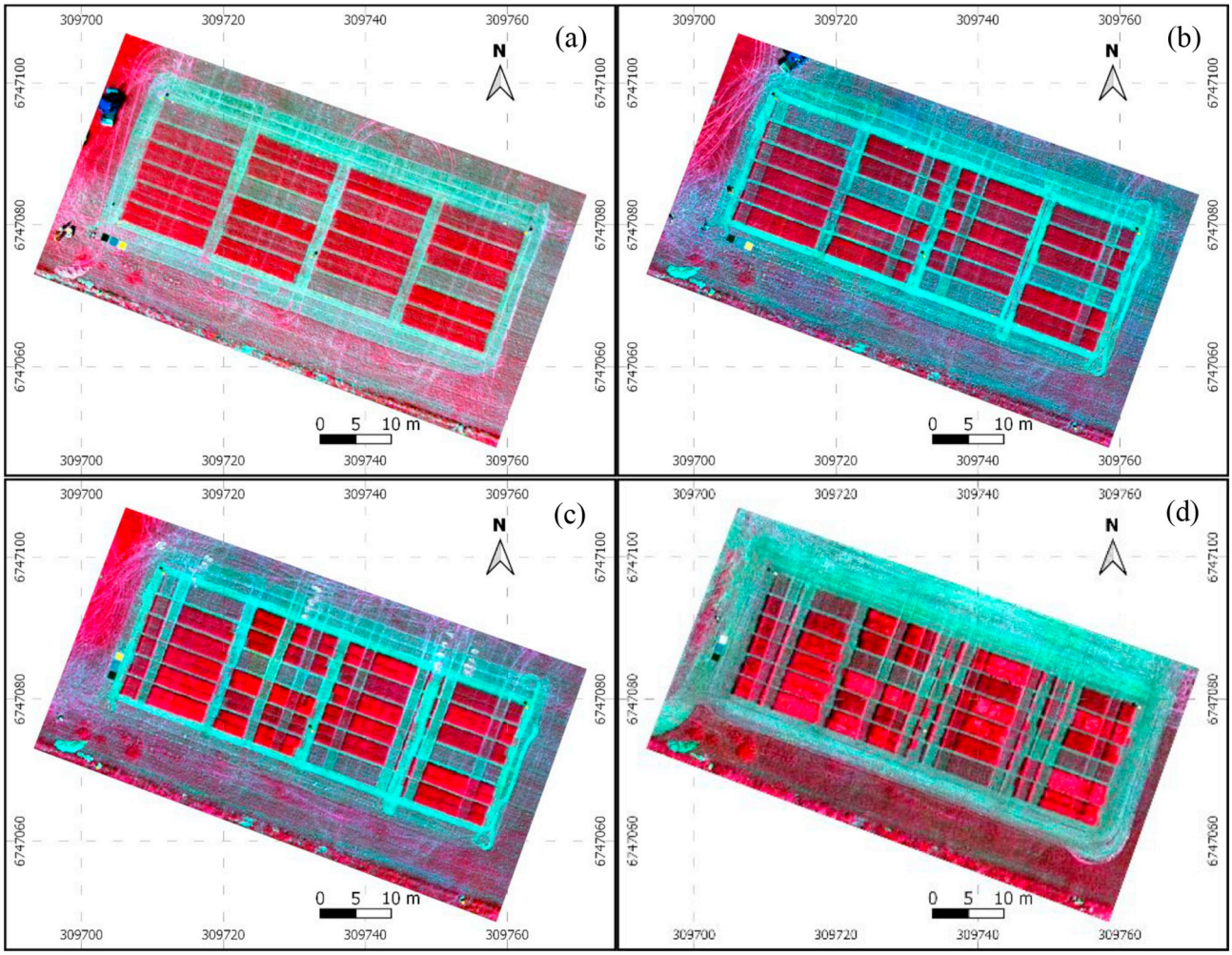

Fig. 5. Orthomosaics for the datasets of the training data site of the primary growth experiment for datasets (a) PG_TR_20170606, (b) PG_TR_20170615, (c) PG_TR_20170619, (d) PG_TR_20170628. Bands: 29 (790.85 nm), 17 (656.34 nm), 6 (545.62 nm).

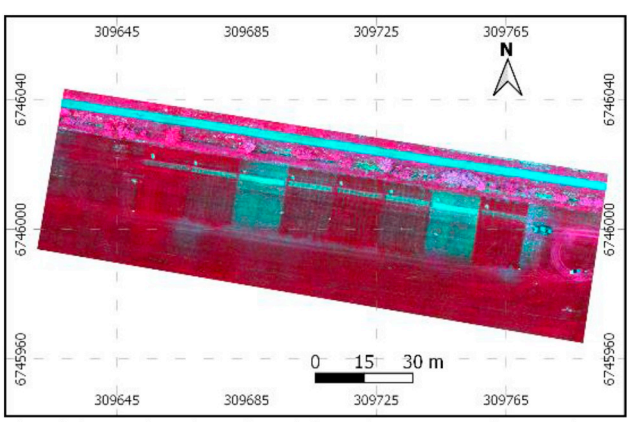

Fig. 6. An orthomosaic of the testing data site of the primary growth experiment PG_TE_20170615. Bands: 29 (790.85 nm), 17 (656.34 nm), 6 (545.62 nm).

hyperspectral images, vegetation indices and CHMs in order to assess the performance of various available sensors with different spectral resolutions. A description of the feature combinations used in our tests is presented in Table 7. The 3D + RGB_b + RGB_i + MS_i set denotes a multispectral camera simulation since it includes RGB bands, and red and NIR spectral bands from the hyperspectral camera (central wavelength L0 = 669.0 nm; full width at half maximum [FWHM] value of 27.0 nm and near infrared L0 = 804.1 nm, FWHM: 28.3 nm). For the MLR estimations, only the feature combination 3D + HS_b + HS_i, representing the hyperspectral sensor, was used.

We built machine-learning estimators for the primary phase (see Section 3.1) and regrowth phase (Section 3.2) due to the differences in the test areas and properties of the crops. For each growth stage, two experimental cases were studied. First, we considered a multitemporal case (Sections 3.1.1 and 3.2.1) where all the dates of the studied growth were used together to estimate different models accounting for the feature sets described in Table 7. Second, the best performing feature set of the multitemporal experiments was used to investigate the estimation of quantity and quality parameters using each date separately (Sections 3.1.2 and 3.1.2).

The quality assessment was quantified by calculating the PCC, RMSE and normalised RMSE (RMSE%) (see the formulas in the work of Viljanen et al., 2018). The leave-one-out cross-validation (LOOCV) method was used to calculate the predicted RMSEs. Additionally, the final RF models for each set of the feature combinations were tested using the external testing data sets of different locations from the training data set. The correlation coefficient of determination, RMSE and RMSE% were also calculated as performance measures between the observed and predicted values of the independent testing data. Table 8 summarises the experiment settings.

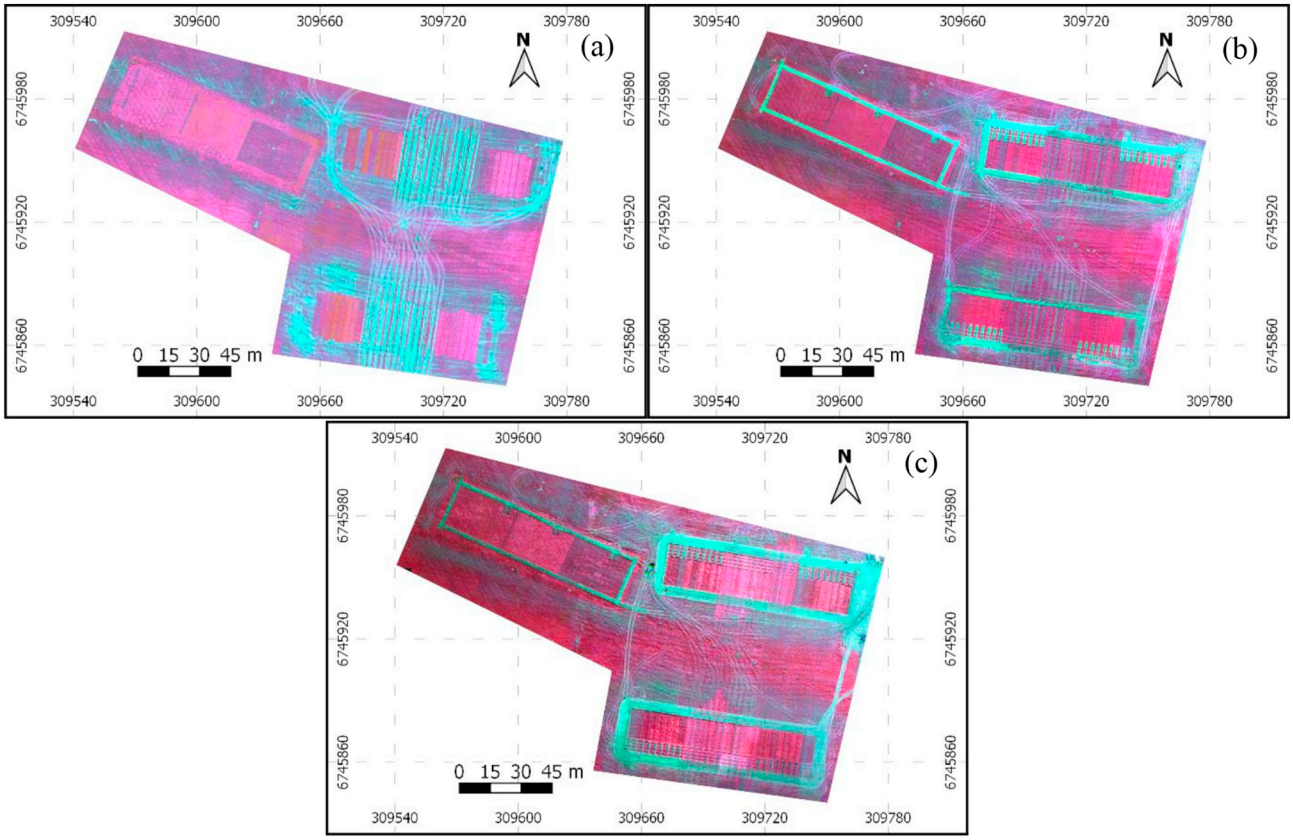

Fig. 7. Orthomosaics for the datasets of the training and testing data sites of the regrowth experiments (a) RG_TR20170724/RG_TE20170724, (b) RG_TR20170803/RG_TE20170803, (c) RG_TR20170814/RG_TE20170814. Bands: 29 (790.85 nm), 17 (656.34 nm), 6 (545.62 nm).

3. Results

3.1. Machine-learning estimators for primary growth

3.1.1. Multi-temporal estimators

Tables 9 and 10 show the results of the RF and MLR models applied to the training and testing data sets.

For the primary growth training datasets, the RF obtained correlations of 0.96–0.98 and RMSE% values of 13.39–16% for biomass estimation within different combinations (Tables 9, 10). Overall, the estimation of the FY was more accurate than the estimation of the DMY. The results were worst when only using 3D features (RMSE%: 23.3% for FY and 21% for DMY; PCC: 0.93). The best results from the RF for FY and DMY were obtained using the feature set 3D + HS_b + HS_i, with PCCs of 0.98 and 0.97 respectively, and RMSE% values of 13.39% and 14.66% respectively. The feature set combining 3D and multispectral features, 3D + RGB_b + RGB_i + MS_i, was only slightly worse with RMSE% of 13.63% for FY and 15.11% for DMY (see Table 9). MLR (3D + HS_b + HS_i) obtained the best accuracy for FY (PCC: 0.98; RMSE%: 11.98%) and the same level for the DMY as with the RF.

Although the poorest RMSE% for FY and DMY estimation in the training experiments, the 3D feature combination performed relatively better than most of the combinations using spectral data with the testing data set, achieving PCCs of 0.97 and 0.94, and RMSE% values of 23.23% and 33.58% for the FY and DMY respectively. The combination 3D + HS_b + HS_i provided the best accuracy of the testing estimations with RMSE% of 20.79% and 23.02% for the FY and DMY respectively. The results with MLR and the feature combination 3D + HS_b + HS_i

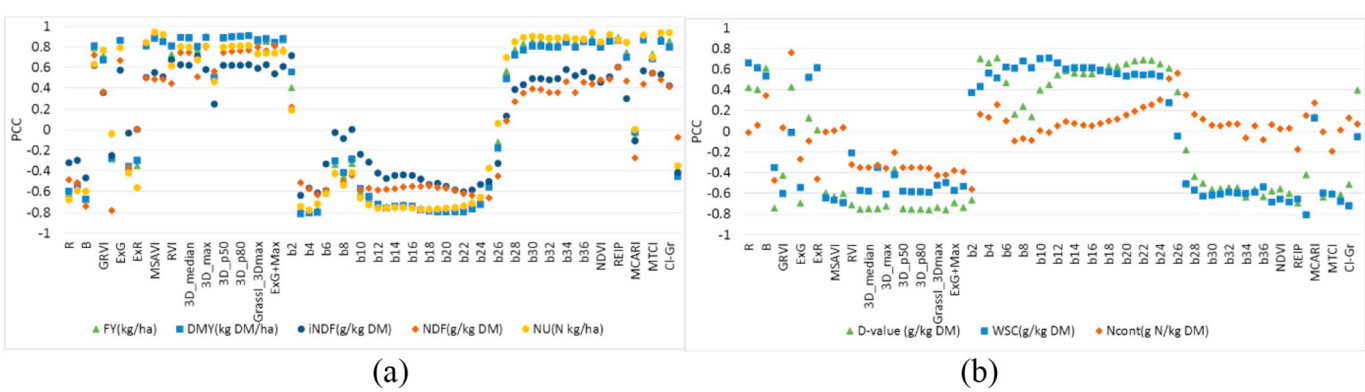

Fig. 8. The Pearson correlation coefficients (PCC) for individual features and physical primary growth measurements of (a) the fresh yield (FY), dry matter yield (DMY), neutral detergent fibre (NDF), indigestible neutral detergent fibre (iNDF) and nitrogen uptake (NU) and (b) the digestible organic matter in dry matter (the D-value), water soluble carbohydrates (WSCs) and nitrogen concentration (Ncont).

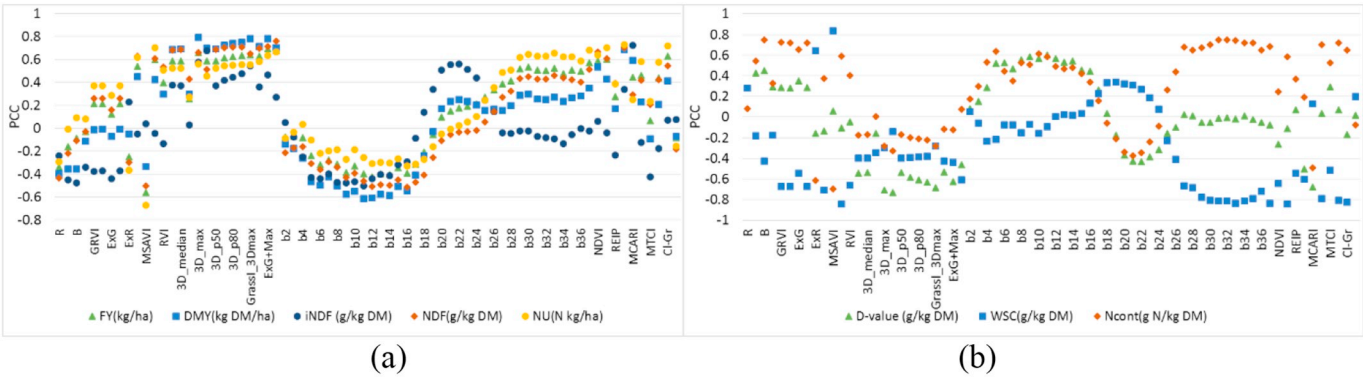

Fig. 9. The Pearson correlation coefficients (PCC) for individual features and physical regrowth measurements of (a) the fresh yield (FY), dry matter yield (DMY), neutral detergent fibre (NDF), indigestible neutral detergent fibre (iNDF) and nitrogen uptake (NU) and (b) the digestible organic matter in dry matter (the D-value), water soluble carbohydrates (WSCs) and nitrogen concentration (Ncont).

Table 7
The labels for the different feature combinations.

Feature combinations	Feature sets included			Case
3D	RGB_3D			3D features from the RGB camera
3D + RGB_b + RGB_i	RGB_3D	RGB_b	RGB_i	3D, spectral and intensity features from the RGB camera
3D + RGB_b + RGB_i + MS_i	RGB_3D	RGB_b	MS_i	3D, spectral and intensity features from a simulated multispectral camera
HS_b + HS_i	HS_i	HS_b		Spectral and indices features from the hyperspectral camera
3D + HS_b + HS_i	HS_i	HS_b	RGB_3D	3D and spectral and indices features from the hyperspectral camera

were clearly poorer than when using the RF.

For the quality estimations with the training datasets, using only 3D features yielded the worst results for all parameters, and hyperspectral features improved these values, as can be seen for 3D + HS_b + HS_i, where the PCCs varied from 0.91 to 0.96 and the RMSE% values varied from 2.11% to 20.73%. The combination 3D + RGB_b + RGB_i + MS_i produced the best (or close to the best) correlations and RMSE%, with PCC of 0.87–0.96 and RMSE% values of 2.76–25.44%. The hyperspectral feature sets 3D + HS_b + HS_i and HS_b + HS_i were best for the estimation of the D-value, iNDF, WSC, Ncont and NU. At its best, the D-value had a PCC of 0.94 and RMSE% of 1.98% (in the HS_b + HS_i test). The addition of 3D features to hyperspectral features (3D + HS_b + HS_i) did not significantly impact on the accuracies obtained for the quality parameters in the HS_b + HS_i data. The D-value and NDF parameters were the parameters with highest level of accuracy from the estimations, with RMSE% values from 1.98% to 3.45% for the D-value and from 2.96% to 5.1% for the NDF. Regarding the MLR(3D + HS_b + HS_i), the best RMSE% values were achieved for the D-value (1.72%), iNDF (16.4%) and WSC (11.98%).

With the testing dataset, the feature set HS_b + HS_i yielded the best accuracy for the D-value with RF having an RMSE% of 1.44% and PCC of 0.81. The MLR(3D + HS_b + HS_i) provided slightly better results with RMSE% of 1.25% and PCC of 0.7. The 3D + RGB_b + RGB_i features provided the highest accuracy in the estimation of NDF (RMSE%: 6.65%). For the Ncont and NU parameters, the 3D + RGB_b + RGB_i + MS_i combination provided the best estimations. The MLR(3D + HS_b + HS_i) resulted in the best RMSE% values for the D-value, iNDF and WSC, compared to the results obtained with the RF.

The relationship between the estimated and measured values for the training and testing results of the 3D + HS_b + HS_i feature set with an RF are plotted in Fig. 10, as well as the absolute RMSEs and the PCC obtained for each parameter. In the training data, the biomass (FY and DMY) was slightly underestimated for higher values (FY > 20,000 g/kg DM; DMY > 4000 g/kg DM). The same can be observed for the Ncont (> 35 g/kg DM). In the testing data, the D-value, NDF and NU were underestimated and the opposite was found for the iNDF and WSC, which were overestimated. Overall, the measured and estimated values presented a very good fit; the correspondences appeared to be the best for the FY, DMY, D-value, Ncont and NU; iNDF, NDF and the WSC appeared to be the most biased values.

3.1.2. *Estimators for each date*

In order to analyse each harvest date of the primary growth

Table 8
A summary of the experiments and results section. RF: random forest; MLR: multiple linear regression; LOOCV: leave-one-out cross-validation.

Data	Section	Experiment	Feature sets	Estimation method	Assessment
Primary growth	3.1.1	Models estimated using all the harvest dates	3D 3D + RGB_b + RGB_i 3D + RGB_b + RGB_i + MS_i HS_b + HS_i 3D + HS_b + HS_i	RF and MLR	LOOCV, independent test data
	3.1.2	One model estimated for each harvest date	3D + HS_b + HS_i	RF	LOOCV
Regrowth	3.2.1	Models estimated using all the harvest dates	3D 3D + RGB_b + RGB_i 3D + RGB_b + RGB_i + MS_i HS_b + HS_i 3D + HS_b + HS_i	RF and MLR	LOOCV, independent test data
	3.2.2	One model estimated for each harvest date	3D + HS_b + HS_i	RF	LOOCV

Table 9
The Pearson correlation coefficient (PCC) of the training data and testing data for the primary growth phase. FY: fresh yield; DMY: dry matter yield; D-value: digestible organic matter in dry matter; iNDF: indigestible neutral detergent fibre; NDF: neutral detergent fibre; WSC: water-soluble carbohydrates; Ncont: nitrogen concentration; NU: nitrogen uptake.

Features	FY	DMY	D-value	iNDF	NDF	WSC	Ncont	NU
Training data PCC								
3D	0.93	0.93	0.78	0.73	0.87	0.67	0.71	0.83
3D + RGB_b + RGB_i	0.97	0.96	0.90	0.85	0.96	0.89	0.93	0.93
3D + RGB_b + RGB_i + MS_i	0.98	0.97	0.90	0.87	0.96	0.90	0.96	0.95
HS_b + HS_i	0.97	0.97	0.94	0.93	0.93	0.91	0.95	0.96
3D + HS_b + HS_i	0.98	0.97	0.93	0.92	0.94	0.91	0.96	0.96
MLR(3D + HS_b + HS_i)	0.98	0.97	0.95	0.95	0.95	0.92	0.93	0.96
Testing data PCC								
3D	0.97	0.94	0.94	0.70	0.56	0.78	−0.75	0.84
3D + RGB_b + RGB_i	0.92	0.84	0.86	0.60	0.57	0.89	0.53	0.94
3D + RGB_b + RGB_i + MS_i	0.95	0.88	0.83	0.67	0.52	0.94	0.85	0.93
HS_b + HS_i	0.83	0.75	0.81	0.87	−0.32	0.88	0.47	0.89
3D + HS_b + HS_i	0.90	0.85	0.93	0.92	−0.07	0.88	0.43	0.89
MLR(3D + HS_b + HS_i)	0.90	0.83	0.70	0.12	0.00	0.96	0.95	0.91

individually, we trained estimators for each date using the RF and feature combinations 3D + RGB_b + RGB_i, 3D + RGB_b + RGB_i + MS_i and 3D + HS_b + HS_i (see Tables 11 and 12) to represent different types of sensors. The FY and DMY quantity parameters obtained similar RMSE% levels for the first, second and fourth harvests while the best estimations were achieved on the third harvest date (RMSE%: 9.9% and 8.27% for the FY and DMY respectively) (see Tables 11 and 12).

The accuracy of the model prediction was relatively higher (mostly on the 15th of June) for all quantity and quality parameters (Fig. 11). The best results for the quality parameters of the D-value, WSC and Ncont were achieved on the second harvest date (PG_TR20170615) with RMSE% values of 0.86%, 7.01% and 5.27% respectively using the 3D + HS_b + HS_i feature set. The quality of the predictions (absolute RMSEs and PCCs) considering the different stages of growth can be observed in Fig. 11. The difference between 3D + RGB_b + RGB_i, 3D + RGB_b + RGB_i + MS_i and 3D + HS_b + HS_i was smaller when estimators were built for each date (Table 12) than for multitemporal models (Table 10), especially with the D-value and NDF. Overall, the accuracies of the estimations were slightly improved for all parameters in comparison to the results for multitemporal models (see Section 3.1.1).

3.2. Machine-learning estimators for regrowth

3.2.1. Multi-temporal estimators

In the grass regrowth experiments, the PCC and RMSE% for biomass estimation using the training data varied from 0.73 to 0.96 and 12.94% to 33.02% respectively (Tables 13 and 14). From the RF tests, the HS_b + HS_i combination obtained the best results for the FY estimation (PCC: 0.94; RMSE%: 17.18%) and for the DMY (PCC: 0.95; RMSE %: 15.23%). However, MLR(3D + HS_b + HS_i) outperformed the RF results both for FY (PCC: 0.96; RMSE%: 12.94%) and for DMY (PCC: 0.96; RMSE%: 13.06%). Similar to the primary growth experiments, the worst accuracies were obtained when using 3D features alone and when using the 3D + RGB_b + RGB_i feature set. For the testing data, the best results were obtained from the 3D + RGB_b + RGB_i + MS_i features (FY: PCC: 0.69 and RMSE%: 26.61%; DMY: PCC: 0.72 and RMSE%: 25.89%).

Regarding the quality parameters in the training data, spectral features also improved the quality of the estimations, and the sets HS_b + HS_i and 3D + HS_b + HS_i provided the best results. Similarly to the primary growth results, the parameters of the D-value (RMSE%: 2.53–3.8%) and NDF (RMSE%: 4.61–5.54%) presented the best accuracies for the regrowth. The RF achieved compatible accuracies and correlations as the best results using MLR and outperformed MLR for

Table 10
The normalised root-mean-square error (RMSE%) of the training data and testing data for the primary growth phase. FY: fresh yield; DMY: dry matter yield; D-value: digestible organic matter in dry matter; iNDF: indigestible neutral detergent fibre; NDF: neutral detergent fibre; WSC: water soluble carbohydrates; Ncont: nitrogen concentration; NU: nitrogen uptake.

Features	FY	DMY	D-value	iNDF	NDF	WSC	Ncont	NU
Training data RMSE%								
3D	23.31	21.08	3.45	34.87	5.10	22.73	24.21	27.55
3D + RGB_b + RGB_i	15.63	16.05	2.48	26.86	2.96	14.14	12.90	18.61
3D + RGB_b + RGB_i + MS_i	13.63	15.11	2.46	25.44	3.00	13.47	10.75	14.90
HS_b + HS_i	14.63	15.24	1.98	19.48	3.70	12.35	10.98	13.93
3D + HS_b + HS_i	13.39	14.66	2.11	20.73	3.53	12.44	10.58	13.56
MLR(3D + HS_b + HS_i)	11.98	15.64	1.72	16.40	3.22	11.98	13.18	14.68
Testing data RMSE%								
3D	23.23	33.58	4.01	82.92	7.45	22.84	37.40	33.31
3D + RGB_b + RGB_i	40.81	50.60	5.29	99.84	6.65	35.82	17.22	25.50
3D + RGB_b + RGB_i + MS_i	24.12	35.72	3.95	78.36	6.71	37.88	12.49	19.02
HS_b + HS_i	36.80	31.56	1.44	37.79	12.87	39.89	19.71	31.30
3D + HS_b + HS_i	20.79	23.02	2.77	66.95	9.32	41.81	17.77	31.23
MLR(3D + HS_b + HS_i)	52.93	36.56	1.25	17.26	18.67	13.25	56.65	25.64

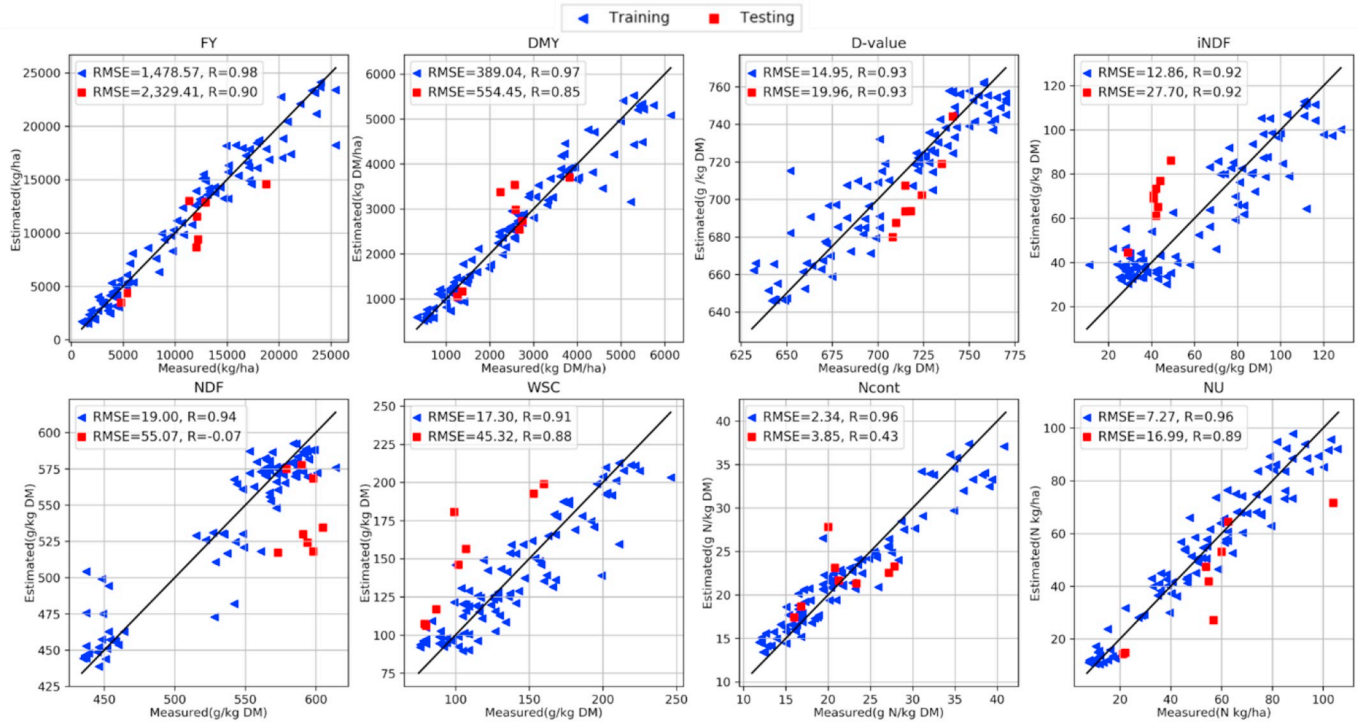

Fig. 10. The relationship between the estimated and measured values for the training and testing data for the primary growth phase using random forest estimation method with the 3D + HS_b + HS_i feature combination. FY: fresh yield; DMY: dry matter yield; D-value: digestible organic matter in dry matter; iNDF: indigestible neutral detergent fibre; NDF: neutral detergent fibre; WSC: water-soluble carbohydrates; Ncont: nitrogen concentration; NU: nitrogen uptake; RMSE: absolute root-mean-square error; R: Pearson correlation coefficient.

Table 11
The Pearson correlation coefficient of the training data for the primary growth phase for each harvesting date using the 3D + HS_b + HS_i feature combination. FY: fresh yield; DMY: dry matter yield; D-value: digestible organic matter in dry matter; iNDF: indigestible neutral detergent fibre; NDF: neutral detergent fibre; WSC: water-soluble carbohydrates; Ncont: nitrogen concentration; NU: nitrogen uptake.

	FY	DMY	D-value	iNDF	NDF	WSC	Ncont	NU
PG_TR20170606								
3D + RGB_b + RGB_i	0.93	0.89	−0.08	−0.02	0.79	0.87	0.82	0.87
3D + RGB_b + RGB_i + MS_i	0.96	0.92	−0.09	−0.04	0.80	0.91	0.88	0.93
3D + HS_b + HS_i	0.95	0.94	−0.10	0.05	0.73	0.93	0.91	0.94
PG_TR20170615								
3D + RGB_b + RGB_i	0.95	0.95	0.85	0.12	0.80	0.97	0.89	0.94
3D + RGB_b + RGB_i + MS_i	0.95	0.95	0.86	0.17	0.81	0.97	0.94	0.95
3D + HS_b + HS_i	0.96	0.95	0.86	0.30	0.79	0.98	0.95	0.96
PG_TR20170619								
3D + RGB_b + RGB_i	0.97	0.98	0.51	0.49	0.68	0.89	0.83	0.97
3D + RGB_b + RGB_i + MS_i	0.97	0.98	0.51	0.47	0.68	0.87	0.83	0.97
3D + HS_b + _i	0.98	0.98	0.55	0.48	0.73	0.91	0.83	0.97
PG_TR20170628								
3D + RGB_b + RGB_i	0.96	0.95	0.76	0.69	0.72	0.86	0.84	0.94
3D + RGB_b + RGB_i + MS_i	0.97	0.95	0.76	0.70	0.73	0.88	0.86	0.95
3D + HS_b + HS_i	0.97	0.95	0.79	0.72	0.74	0.88	0.88	0.95

the D-value, iNDF and NDF. For the testing data, the sets 3D and 3D + RGB_b + RGB_i outperformed the other combinations in the estimations of the D-value and iNDF. MLR(3D + HS_b + HS_i) achieved better results than the RF for most of the quality parameters.

The distributions of the attributes predicted in the training and testing data, using RF with the 3D + HS_b + HS_i feature set versus the reference values of the field samples are presented in Fig. 12. It can be seen that the D-value was overestimated for the testing data and the predicted values for the training data were underestimated for the high values. In particular, the iNDF and NU of the test datasets were underestimated.

3.2.2. Estimators for each date

RF models with 3D, RGB, multispectral and hyperspectral features were used to estimate the quantity and quality of regrowth data for individual dates. The FY parameter presented similar RMSE% values for each separate date and the best results were found on the third harvesting date (RG_TR20170814) (PCC: 0.95; RMSE%: 14.45%). For the DMY, the second harvesting date (RG_TR20170803) yielded the best accuracies (PCC: 0.97; RMSE%: 9.97%) (Tables 15 and 16). Each feature set achieved a similar level of accuracy for each date, but 3D + HS_b + HS_i provided the best accuracies for the biomass and quality parameters on all dates. Overall, the best accuracies for quality parameters were on the second harvesting date (RG_TR20170803).

Table 12
The normalised root-mean-square error of the training data for the primary growth phase for each harvesting date using the 3D + HS_b + HS_i feature combination. FY: fresh yield; DMY: dry matter yield; D-value: digestible organic matter in dry matter; iNDF: indigestible neutral detergent fibre; NDF: neutral detergent fibre; WSC: water soluble carbohydrates; Ncont: nitrogen concentration; NU: nitrogen uptake.

	FY	DMY	D-value	iNDF	NDF	WSC	Ncont	NU
PG_TR20170606								
3D + RGB_b + RGB_i	14.27	14.92	1.65	22.82	1.19	11.99	9.81	20.71
3D + RGB_b + RGB_i + MS_i	11.10	12.49	1.66	22.99	1.17	10.28	8.00	16.13
3D + HS_b + HS_i	11.38	11.24	1.76	23.24	1.33	9.14	6.97	14.46
PG_TR20170615								
3D + RGB_b + RGB_i	12.82	10.65	0.89	21.25	1.78	7.75	7.79	14.78
3D + RGB_b + RGB_i + MS_i	12.27	10.75	0.88	20.94	1.75	7.75	5.94	13.72
3D + HS_b + HS_i	11.66	10.39	0.86	19.86	1.83	7.01	5.27	12.36
PG_TR20170619								
3D + RGB_b + RGB_i	11.08	8.89	2.26	14.67	2.97	14.46	8.51	11.92
3D + RGB_b + RGB_i + MS_i	10.50	9.05	2.25	14.80	2.98	15.30	8.45	12.30
3D + HS_b + HS_i	9.90	8.27	2.14	15.10	2.73	13.04	8.54	12.45
PG_TR20170628								
3D + RGB_b + RGB_i	12.74	11.72	1.75	9.27	2.68	13.58	8.48	15.83
3D + RGB_b + RGB_i + MS_i	10.88	11.46	1.74	9.12	2.62	12.52	8.02	14.12
3D + HS_b + HS_i	11.48	11.50	1.66	8.93	2.58	12.81	7.28	14.46

Compared with the primary growth results (see Section 3.1.2), the regrowth results showed higher RMSE% values for both quantity and quality parameters. The relationship between the estimated and measured values for the training data of the regrowth stage for each date shows that for the data RG_TR20170814, the DMY, Ncont and NU were underestimated for high values (see Fig. 13).

4. Discussion

In order to investigate the potential of drone-based photogrammetry and spectral imaging in silage grass sward quality and quantity estimation, controlled grass sward trial sites were established for the primary growth and regrowth phases of grass, and these were used to develop models for estimating grass parameters using drone-based remote-sensing data. The accuracies of estimating the quantity and quality of the yield were at similar levels to those obtained in previous studies using conventional techniques (Rinne, 2000; Kuoppala, 2010; Nissinen et al., 2010). The representativeness of the datasets used in this study for practical farming situations differed. In the primary growth training dataset, harvest for silage at the first reference measurements (on the 6th of June) was too early, and the last harvesting date (the 28th of June) was too late as the stand was heading heavily and was also lodged at the highest nitrogen application rates. The harvest dates of the 15th and 19th of June represented well the

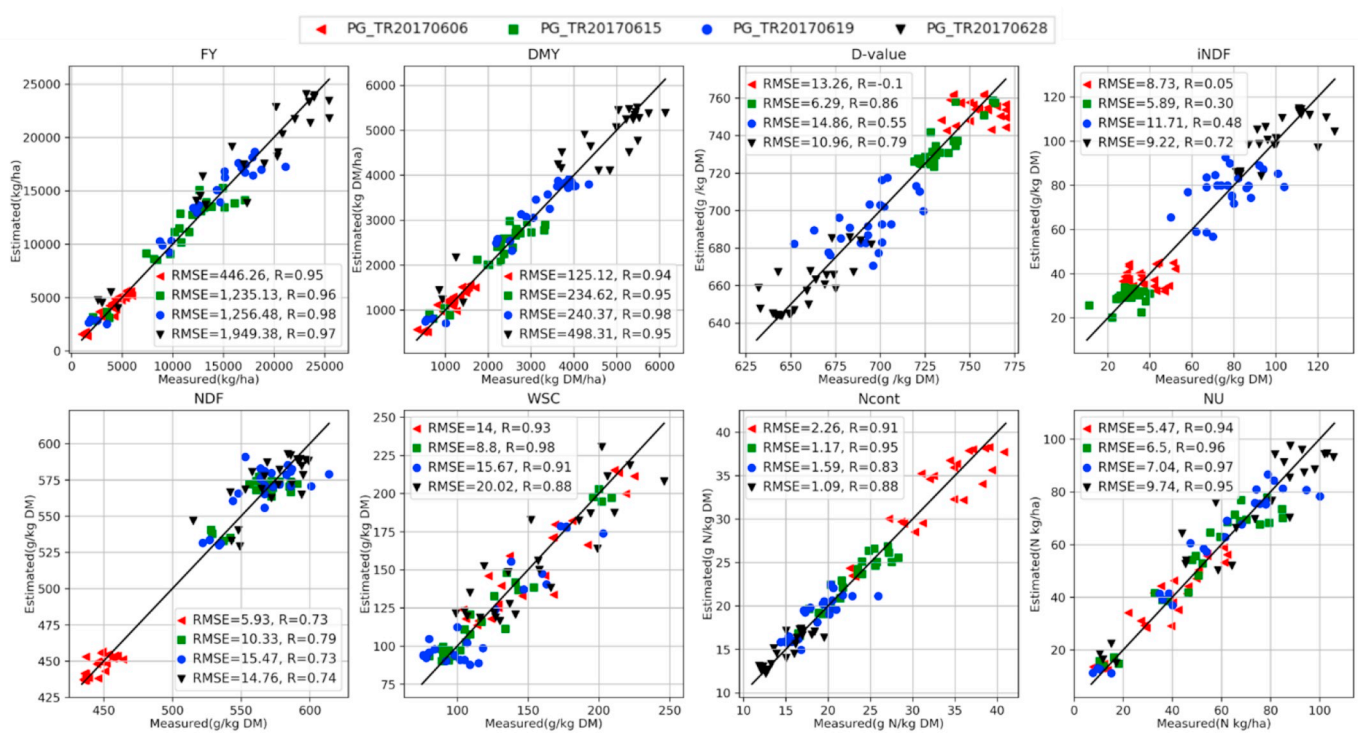

Fig. 11. The relationship between the estimated and measured values for the training data for the primary growth phase, separated by date using random forest estimation method with the 3D + HS_b + HS_i feature combination. FY: fresh yield; DMY: dry matter yield; D-value: digestible organic matter in dry matter; iNDF: indigestible neutral detergent fibre; NDF: neutral detergent fibre; WSC: water-soluble carbohydrates; Ncont: nitrogen concentration; NU: nitrogen uptake; RMSE: absolute root-mean-square error; R: Pearson correlation coefficient.

Table 13
The Pearson correlation coefficient (PCC) of the training data and the testing data for the regrowth phase. FY: fresh yield; DMY: dry matter yield; D-value: digestible organic matter in dry matter; iNDF: indigestible neutral detergent fibre; NDF: neutral detergent fibre; WSC: water-soluble carbohydrates; Ncont: nitrogen concentration; NU: nitrogen uptake.

Features	FY	DMY	D-value	iNDF	NDF	WSC	Ncont	NU
Training data PCC								
3D	0.73	0.80	0.65	0.55	0.73	0.60	0.39	0.66
3D + RGB_b + RGB_i	0.83	0.88	0.76	0.71	0.78	0.87	0.88	0.83
3D + RGB_b + RGB_i + MS_i	0.87	0.90	0.79	0.75	0.78	0.88	0.88	0.86
HS_b + HS_i	0.94	0.95	0.86	0.85	0.82	0.88	0.84	0.90
3D + HS_b + HS_i	0.94	0.94	0.86	0.84	0.81	0.88	0.84	0.90
MLR(3D + HS_b + HS_i)	0.96	0.96	0.86	0.83	0.79	0.91	0.89	0.92
Testing data								
3D	0.51	0.62	0.86	0.80	0.83	−0.22	−0.38	0.28
3D + RGB_b + RGB_i	0.54	0.70	0.91	0.88	0.84	0.42	0.76	0.39
3D + RGB_b + RGB_i + MS_i	0.69	0.72	0.92	0.88	0.86	0.94	0.85	0.69
HS_b + HS_i	0.84	0.84	0.82	0.66	0.84	0.76	0.88	0.84
3D + HS_b + HS_i	0.85	0.86	0.80	0.68	0.93	0.76	0.88	0.87
MLR(3D + HS_b + HS_i)	0.83	0.66	0.91	0.92	0.90	0.86	0.94	0.92

ordinary primary growth harvest situation in Finland, particularly at 75–125 kg N ha^{-1} rates. In the regrowth data, the harvest taken on the 26th of July and the 1st of August represented the best practical silage production situation. On the last harvest date (the 15th of August), the lowest leaves in the densest swards with high nitrogen application rates had started to die, which resulted in poor digestibility in the reference analyses (Virkajärvi et al., 2012).

We separated the estimation processes of the primary and regrowth phases due to the differences in the test areas and in the properties of the crops. The best (or close to the best) quantity and quality estimations for the training data on primary growth were obtained when combining 3D features, hyperspectral bands and vegetation indices. In this case, when using LOOCV estimation to assess the RF model, the correlations and RMSE% (RMSE) were, respectively, at best 0.98 and 13.4% (1479 kg/ha) for the FY, and 0.97 and 14.7% (389 kg/DM) for the DMY, and for the quality parameters, the PCCs and RMSE% values were 0.91–0.96 and 2.11–20.73% respectively. At best, the D-value was estimated with an RMSE% (RMSE) of 1.98% (14 g/kg DM) using hyperspectral bands and vegetation indices (HS_b + HS_i). In the testing data of the primary growth, the D-value was estimated with the same level of accuracy as that obtained in the training data results using hyperspectral data. However, for other parameters the estimation errors increased, most likely due to the differences between the training and testing areas. The findings for the regrowth areas were aligned with the primary growth areas, but with smaller PCC values and higher RMSE values. Despite the higher performance of hyperspectral data in LOOCV validation, in some cases the multispectral feature set outperformed the hyperspectral set for the testing data for both the primary growth and regrowth. The results of the HS_b + HS_i and 3D + HS_b + HS_i sets were similar for most of the cases in the primary growth and regrowth; however, the use of 3D features significantly improved the biomass estimation in the primary growth but not in the regrowth. Overall, the MLR and RF provided relatively similar results.

Our quality parameters results were at similar levels as those found in the results of Pullanagari et al. (2012) and Pullanagari et al. (2018). Pullanagari et al. (2012) investigated the use of a hand-held hyperspectral sensor (with a 500–2400 nm range) to estimate several pasture quality parameters using partial least squares regression. The R^2 and RMSE% of the LOOCV were, respectively, 0.82 and 10.10% for CP, 0.77 and 9.7% for NDF and 0.83 and 5.3% for OMD. For the validation data, the R^2 and RMSE% were, respectively, 0.78 and 11.32% for CP, 0.75 and 10.56% for NDF and 0.83 and 5.14% for OMD. Pullanagari et al. (2018) studied RF using spectral features from a pushbroom hyperspectral camera and topographical features in order to estimate the CP and ME; at best they achieved an R^2 of 0.8 and RMSE% of 1.68% for CP, and an R^2 of 0.78 and RMSE of 0.61 MJ/kg DM for ME.

The models were also estimated for each harvest date separately. Within the primary growth phase, the accuracies of biomass estimation were similar for each date and the best values were obtained in the third harvest, which was close to the optimal harvest date. For all quantity and quality parameters of the primary growth, the accuracies of the estimations were better when the four harvests were separated.

Table 14
The normalised root-mean-square errors (RMSE%) of the training data and the testing data for the regrowth phase. FY: fresh yield; DMY: dry matter yield; D-value: digestible organic matter in dry matter; iNDF: indigestible neutral detergent fibre; NDF: neutral detergent fibre; WSC: water-soluble carbohydrates; Ncont: nitrogen concentration; NU: nitrogen uptake.

Features	FY	DMY	D-value	iNDF	NDF	WSC	Ncont	NU
Training data RMSE%								
3D	33.02	27.06	3.79	39.00	5.54	37.85	22.70	34.66
3D + RGB_b + RGB_i	26.79	21.19	3.25	32.55	5.10	22.98	11.45	25.69
3D + RGB_b + RGB_i + MS_i	23.66	19.61	3.05	30.58	5.08	22.62	11.65	23.64
HS_b + HS_i	17.18	15.23	2.57	24.33	4.61	22.39	13.03	20.28
3D + HS_b + HS_i	17.24	16.08	2.53	24.77	4.70	21.96	12.93	20.36
MLR(3D + HS_b + HS_i)	12.94	13.06	2.58	25.72	5.07	19.31	11.20	18.34
Testing data RMSE%								
3D	43.67	34.34	2.41	15.29	5.79	50.56	26.29	46.47
3D + RGB_b + RGB_i	36.40	27.82	2.49	24.17	4.20	32.58	24.60	34.49
3D + RGB_b + RGB_i + MS_i	26.61	25.89	2.81	27.03	3.63	16.96	19.01	26.33
HS_b + HS_i	29.21	30.73	4.86	41.37	4.00	28.43	13.99	29.29
3D + HS_b + HS_i	30.60	30.75	4.89	41.24	2.49	26.81	13.52	30.42
MLR(3D + HS_b + HS_i)	26.29	41.46	4.82	21.74	4.72	19.62	11.80	17.57

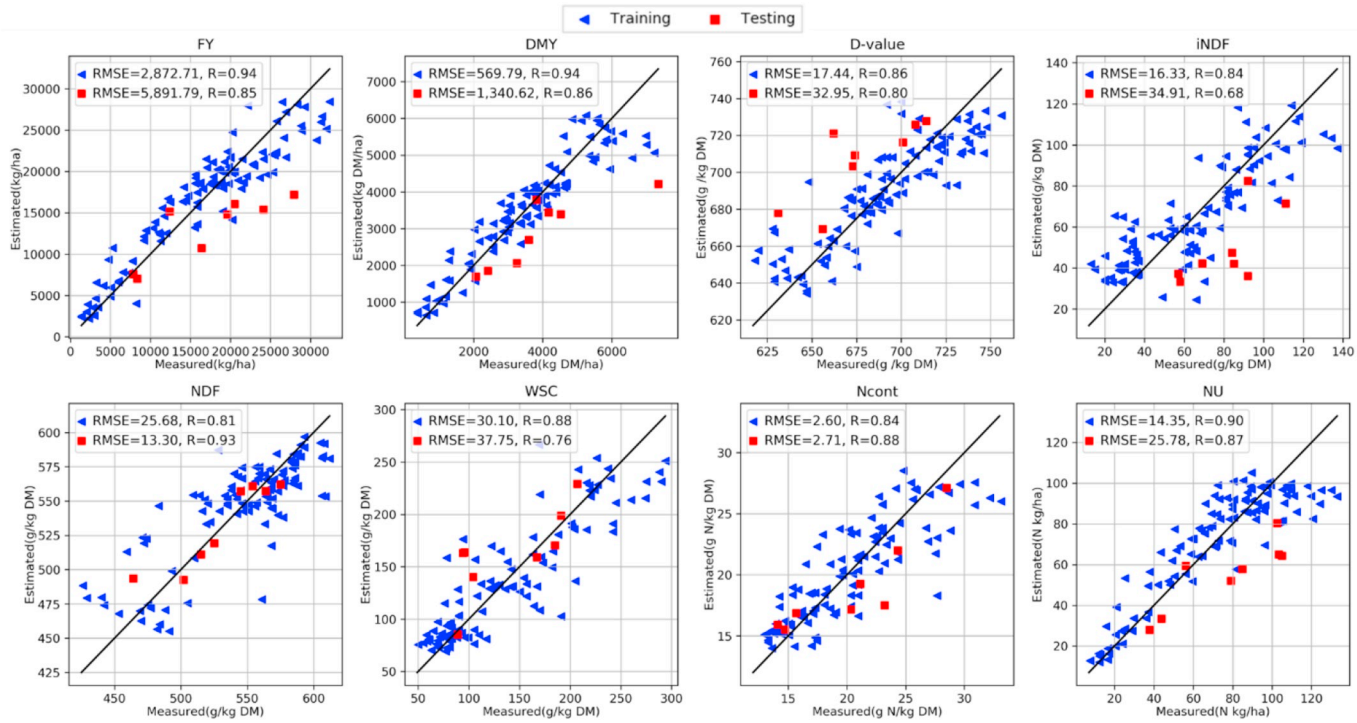

Fig. 12. The relationship between estimated and measured values for the training and testing data for the regrowth phase using random forest estimation method with the 3D + HS_b + HS_i feature combination. FY: fresh yield; DMY: dry matter yield; D-value: digestible organic matter in dry matter; iNDF: indigestible neutral detergent fibre; NDF: neutral detergent fibre; WSC: water-soluble carbohydrates; Ncont: nitrogen concentration; NU: nitrogen uptake; RMSE: absolute root mean square error; R: Pearson correlation coefficient.

However, when all the samples of the three harvests from the regrowth phase were used in the training data (see Tables 13 and 14), the estimations achieved similar values compared to the results for each date when separated (see Tables 15 and 16). In the study carried out by Zheng and Chen (2018), the best estimates were obtained using all dates together; from using MLR, the obtained correlations' R^2 were 0.78, 0.84 and 0.76 for the yield, NDF, and CP respectively, and using the PLSR model, the R^2 were 0.79, 0.80 and 0.77 for the yield, NDF and CP respectively.

One reason for the differences of the results when compared with the combined and individual date datasets might be the remaining inaccuracies in the remote-sensing data calibration. Great effort was applied in the radiometric calibration of the datasets that were captured under varying illumination conditions, but further improvements might be obtained by improving the calibration approaches, for example, by utilising calibrated irradiance sensors and improved spectral calibration (Suomalainen et al., 2018, Aasen et al., 2018). The spectral and 3D features were extracted in separate processes; however, this could be improved by utilising multi-view spectral analysis to generate a spectral DSM (Oliveira et al., 2018; Roosjen et al., 2018). Also, the challenges of the vegetation characteristics during the first and last harvests in the primary growth cases might have reduced the performance. The results indicate that the approach is highly promising, but further studies are needed, for example, in order to investigate the requirements for data calibration and to develop more general estimators.

The NIR-based vegetation indices have provided superior results in comparison with RGB-based vegetation indices in studies on the estimation of crop biomass (Tilly et al., 2015). Bareth and Schellberg (2018) pointed out that the spectral analysis of calibrated RGB imagery for the estimation process has not been fully compared to multispectral and hyperspectral data. We evaluated the performance of 3D data and RGB, multispectral and hyperspectral sensors in the estimation process.

Table 15
The Pearson correlation coefficients of the training data for the regrowth phase for each harvesting date using random forest estimation method with the 3D + HS_b + HS_i feature combination. FY: fresh yield; DMY: dry matter yield; D-value: digestible organic matter in dry matter; iNDF: indigestible neutral detergent fibre; NDF: neutral detergent fibre; WSC: water-soluble carbohydrates; Ncont: nitrogen concentration; NU: nitrogen uptake.

	FY	DMY	D-value	iNDF	NDF	WSC	Ncont	NU
RG_TR20170724								
3D + RGB_b + RGB_i	0.89	0.91	0.52	0.13	0.79	0.88	0.67	0.83
3D + RGB_b + RGB_i + MS_i	0.90	0.93	0.52	0.07	0.78	0.87	0.66	0.83
3D + HS_b + HS_i	0.94	0.95	0.69	0.55	0.76	0.85	0.63	0.89
RG_TR20170803								
3D + RGB_b + RGB_i	0.89	0.93	0.62	0.48	0.82	0.92	0.87	0.91
3D + RGB_b + RGB_i + MS_i	0.93	0.96	0.75	0.60	0.85	0.96	0.88	0.93
3D + HS_b + HS_i	0.92	0.97	0.80	0.72	0.89	0.95	0.75	0.91
RG_TR20170814								
3D + RGB_b + RGB_i	0.83	0.83	0.55	0.36	0.71	0.75	0.38	0.81
3D + RGB_b + RGB_i + MS_i	0.94	0.90	0.63	0.53	0.73	0.77	0.48	0.89
3D + HS_b + HS_i	0.95	0.90	0.63	0.52	0.72	0.74	0.48	0.90

Table 16
The normalised root mean square error of the training data for the regrowth phase for each harvesting date using random forest with the 3D + HS_b + HS_i feature combination. FY: fresh yield; DMY: dry matter yield; D-value: digestible organic matter in dry matter; iNDF: indigestible neutral detergent fibre; NDF: neutral detergent fibre; WSC: water-soluble carbohydrates; Ncont: nitrogen concentration; NU: nitrogen uptake.

	FY	DMY	D-value	iNDF	NDF	WSC	Ncont	NU
RG_TR20170724								
3D + RGB_b + RGB_i	22.44	16.41	2.49	45.10	4.22	25.29	12.95	28.15
3D + RGB_b + RGB_i + MS_i	21.71	15.25	2.48	46.17	4.28	26.10	12.98	28.35
3D + HS_b + HS_i	16.29	13.20	2.09	36.05	4.49	27.49	13.46	23.05
RG_TR20170803								
3D + RGB_b + RGB_i	20.53	13.78	2.68	33.12	4.93	20.11	8.45	20.07
3D + RGB_b + RGB_i + MS_i	16.96	11.29	2.27	30.09	4.45	14.21	8.31	17.40
3D + _b + HS_i	17.19	9.97	2.07	25.76	3.86	15.67	10.93	18.99
RG_TR2017h0814								
3D + RGB_b + RGB_i	25.00	19.60	3.06	17.28	5.78	22.61	12.80	22.17
3D + RGB_b + RGB_i + MS_i	16.32	15.56	2.84	15.61	5.55	22.17	12.12	17.63
3D + HS_b + HS_i	14.45	15.64	2.84	15.95	5.65	23.02	12.15	16.47

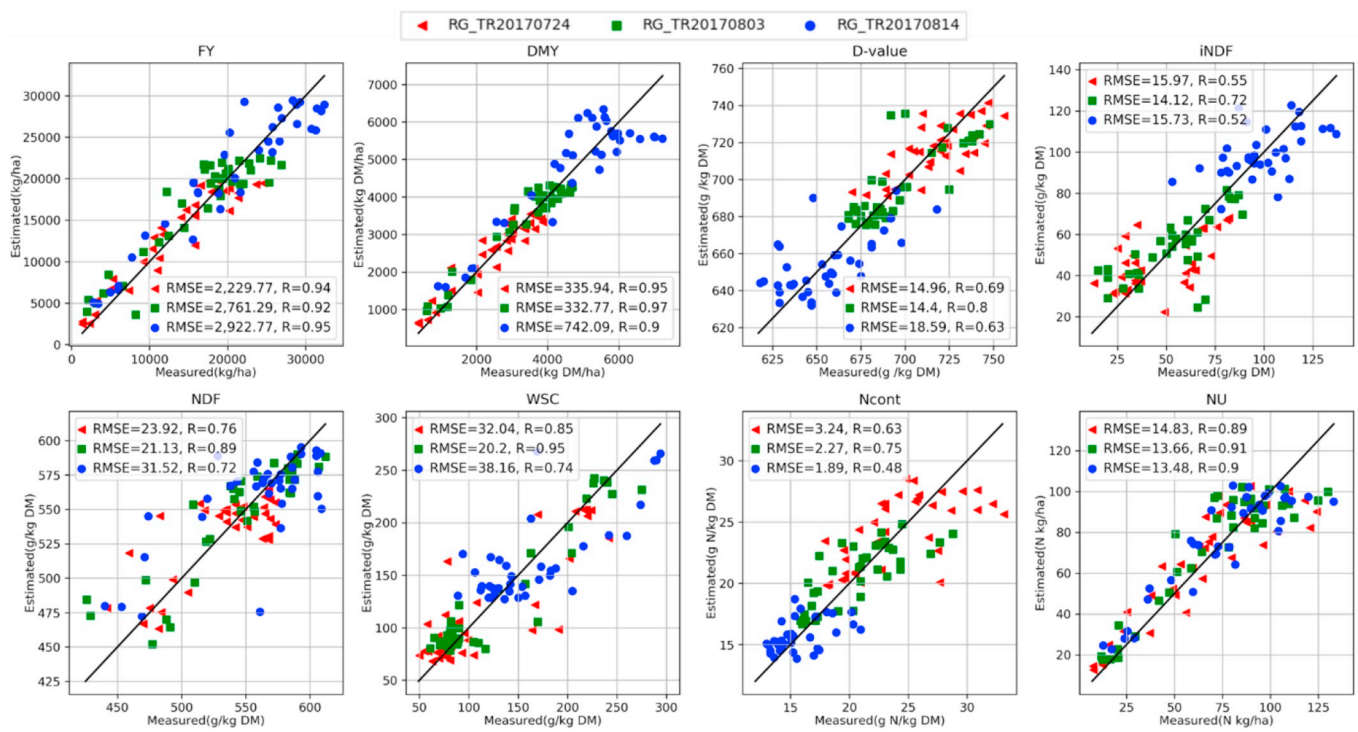

Fig. 13. The relationship between the estimated and measured values for the training data for the regrowth phase separated by date using a random forest with the 3D + HS_b + HS_i feature combination. FY: fresh yield; DMY: dry matter yield; D-value: digestible organic matter in dry matter; iNDF: indigestible neutral detergent fibre; NDF: neutral detergent fibre; WSC: water-soluble carbohydrates; Ncont: nitrogen concentration; NU: nitrogen uptake; RMSE: absolute root mean square error; R: Pearson correlation coefficient.

The estimations using RGB bands (RGB_b), RGB indices (RGB_i) and 3D data (3D + RGB_b + RGB_i) presented compatible results with the multispectral case (3D + RGB_b + RGB_i + MS_i) for the D-value and NDF estimations of the primary growth data and regrowth. However, in general the more spectral features were used, the more accurate the estimation of the quantity and quality attributes became. This led to better overall accuracies using hyperspectral feature combinations, which was even more accentuated in the biomass estimations. The multispectral features combined with 3D features presented results similar to the hyperspectral combinations for D-value, NDF and Ncont estimations in both primary growth and regrowth data. Yue et al. (2018) also obtained better RF estimates of winter wheat's above-ground biomass when combining height and vegetation indices than when using only vegetation indices or only crop height. The authors also used a hyperspectral frame camera and RGB camera mounted on a drone and obtained R^2 of 0.83 and RMSE% of 10.47% for the training data of above-ground biomass.

Utilising drones for predicting the FY and DMY provides valuable information for grazing management that can be used to set stocking rates in order to provide the desired herbage allowance (Virkajärvi, 1999) without rising plate meters, as presented by Bareth and Schellberg (2018). Together with Ncont, DMY facilitates fertiliser application considerations. This study shows that these parameters can be estimated using drone remote sensing with a suitable degree of accuracy. It is important to estimate other quality parameters, in particular the D-value, especially in silage making, since they directly affect the milk production and thus the profitability of the farm (Rinne et al., 1999). In Finland, the D-value is reduced by 5 g/kg DM a day or at an even faster rate during the fastest development period in primary growth; thus, the right timing of harvesting is crucial (Rinne, 2000). Huhtanen et al. (2006) studied various forage evaluation methods to predict D-values and they set the goal of reducing the prediction error

of the D-value to below 15 g/kg DM. The achieved accuracy of our study was 10 g/kg DM in the testing data for the primary growth, which indicates that we can find the optimal harvesting time with 2–3 day accuracy using drone-based hyperspectral imaging and photogrammetry.

The ability to reveal spatial differences in the yield and quality within a field can assist farmers learning from the factors affecting their grassland production. In addition, carrying out on-farm trials can be easier than with the conventional yield-measuring methods. The use of the double sampling technique described by 't Mannetje (2000) for non-destructive methods could be applied to on-farm trials utilising remote sensing. This would include the accurate determination of the DM yield in a few samples (reference data) and the utilisation of drone data from large numbers of trial plots including the reference plots. Jointly utilising the information from grass growth models would help predict, for example, the D-value development and provide further information on the spatial variation in the field by using drone-obtained data (Hyrkäs et al., 2016; Korhonen et al., 2018; Persson et al., 2019). For example, in round-bale harvesting, drone-based data on the variation in D-values within a field could facilitate the identification of the quality of individual bales and facilitate their use accordingly.

5. Conclusions

This study presented the first comprehensive assessment of the potential of drone-based spectral remote sensing and photogrammetry for estimating the biomass and quality parameters of grass swards for silage production. Models were trained using RF- and MLR-based machine learning technologies. The results showed that drone-based remote sensing could be used to predict the yield quantity and quality with an adequate degree of accuracy and to study the spatial differences within a field and between different fields, thus indicating great potential for remote sensing and drones to support the management of silage production for animal feeding. Further studies on cost-efficient sensors, data calibration, the most suitable machine learning techniques and more comprehensive training data will be necessary in order to develop procedures for practical use. Studies using annual harvest data will be valuable in order to assess the performance of the estimators in practical conditions. In comparison to traditional field measurements using rising plate meters, for example, and NIRS analytics, the advantages of a drone-based approach include the potential for automation and real-time measurements, as well as the potential for providing complete spatial coverage of the estimates over the entire field.

CRediT authorship contribution statement

Raquel Alves Oliveira: Investigation, Formal analysis, Writing - original draft, Writing - review & editing. **Roope Näsi:** Investigation, Formal analysis, Writing - original draft, Writing - review & editing. **Oiva Niemeläinen**: Methodology, Formal analysis, Writing - original draft, Writing - review & editing. **Laura Nyholm**: Formal analysis, Writing - review & editing. **Katja Alhonoja**: Formal analysis, Writing - review & editing. **Jere Kaivosoja**: Funding acquisition, Methodology, Formal analysis, Writing - review & editing. **Lauri Jauhiainen**: Formal analysis, Writing - review & editing. **Niko Viljanen**: Investigation, Writing - review & editing. **Somayeh Nezami**: Investigation, Writing - review & editing. **Lauri Markelin**: Investigation, Writing - review & editing. **Teemu Hakala**: Investigation, Writing - review & editing. **Eija Honkavaara**: Project administration, Funding acquisition, Methodology, Formal analysis, Writing - original draft, Writing - review & editing.

Declaration of competing interest

The authors declare that they have no known competing financial interests or personal relationships that could have appeared to influence the work reported in this paper.

Acknowledgements

This research was supported by the Business Finland DroneKnowledge project (Dnro 1617/31/2016) and the ICT Agri ERA-NET 2015 Enabling precision farming project GrassQ-Development of ground-based and Remote Sensing, automated 'real-time' grass quality measurement to enhance grassland management information platforms (Project ID: 35779). We are grateful to the project NESTERAVINNE and Mr. Petri Kapuinen for allowing additional sampling of the experiment.

References

Aasen, H., Honkavaara, E., Lucieer, A., Zarco-Tejada, P.J., 2018. Quantitative remote sensing at ultra-high resolution with UAV spectroscopy: a review of sensor technology, measurement procedures, and data correction workflows. Remote Sens. 10, 1091. https://doi.org/10.3390/rs10071091.

Aastveit, A.H., Marum, P., 1989. Accuracy of near infrared reflectance spectroscopy in the determination of IVDMD in forage. Nor. J. Agric. Sci. 3, 211–219.

Akaike, H., 1974. A new look at the statistical model identification. IEEE Trans. Autom. Control 19, 716–723. https://doi.org/10.1109/TAC.1974.1100705.

Ali, I., Cawkwell, F., Dwyer, E., Barrett, B., Green, S., 2016. Satellite remote sensing of grasslands: from observation to management. J. Plant Ecol. 9 (6), 649–671. https://doi.org/10.1093/jpe/rtw005.

Bareth, G., Schellberg, J., 2018. Replacing manual rising plate meter measurements with low-cost UAV-derived sward height data in grassland for spatial monitoring. PFG. Journal of Photogrammetry, Remote Sensing and Geoinformation Science. https://doi.org/10.1007/s41064-018-0055-2.

Bareth, G., Bolten, A., Hollberg, J., Aasen, H., Burkart, A., Schellberg, J., 2015. Feasibility Study of Using Non-calibrated UAV-based RGB Imagery for Grassland Monitoring: Case Study at the Rengen Long-term Grassland Experiment (RGE), Germany. DGPF Tag. 24. pp. 1–7.

Belgiu, M., Drăguţ, L., 2016. Random forest in remote sensing: a review of applications and future directions. ISPRS J. Photogramm. Remote Sens. 114, 24–31. https://doi.org/10.1016/j.isprsjprs.2016.01.011.

Bendig, J., Bolten, A., Bennertz, S., Broscheit, J., Eichfuss, S., Bareth, G., 2014. Estimating biomass of barley using crop surface models (CSMs) derived from UAV-based RGB imaging. Remote Sens. 6 (11), 10395–10412. https://doi.org/10.3390/rs61110395.

Bendig, J., Yu, K., Aasen, H., Bolten, A., Bennertz, S., Broscheit, J., Gnyp, M.L., Bareth, G., 2015. Combining UAV-based plant height from crop surface models, visible, and near infrared vegetation indices for biomass monitoring in barley. Int. J. Appl. Earth Obs. Geoinf. 39, 79–87. https://doi.org/10.1016/j.jag.2015.02.012.

Berni, J.A.J., Zarco-Tejada, P.J., Suarez, L., Fereres, E., 2009. Thermal and narrowband multispectral remote sensing for vegetation monitoring from an unmanned aerial vehicle. IEEE Trans. Geosci. Remote Sens. 47, 722–738. https://doi.org/10.1109/TGRS.2008.2010457.

Breiman, L., 2001. Random forests. Mach. Learn. 45, 5–32. https://doi.org/10.1023/A:1010933404324.

Candiago, S., Remondino, F., De Giglio, M., Dubbini, M., Gattelli, M., 2015. Evaluating multispectral images and vegetation indices for precision farming applications from UAV images. Remote Sens. 7, 4026–4047. https://doi.org/10.3390/rs70404026.

Capolupo, A., Kooistra, L., Berendonk, C., Boccia, L., Suomalainen, J., 2015. Estimating plant traits of grasslands from UAV-acquired hyperspectral images: a comparison of statistical approaches. ISPRS Int. J. Geo-Inf. 4, 2792–2820. https://doi.org/10.3390/ijgi4042792.

Dash, J., Curran, P.J., 2004. The MERIS terrestrial chlorophyll index. Int. J. Remote Sens. 25, 5403–5413. https://doi.org/10.1080/0143116042000274015.

Daughtry, C.S.T., Walthall, C.L., Kim, M.S., de Colstoun, E.B., McMurtrey, J.E., 2000. Estimating corn leaf chlorophyll concentration from leaf and canopy reflectance. Remote Sens. Environ. 74, 229–239. https://doi.org/10.1016/S0034-4257(00)00113-9.

Geipel, J., Link, J., Wirwahn, J.A., Claupein, W., 2016. A programmable aerial multispectral camera system for in-season crop biomass and nitrogen content estimation. Agriculture 6 (1), 4. https://doi.org/10.3390/agriculture6010004.

Gitelson, A.A., Kaufman, Y.J., Merzlyak, M.N., 1996. Use of a green channel in remote sensing of global vegetation from EOS-MODIS. Remote Sens. Environ. 58, 289–298. https://doi.org/10.1016/S0034-4257(96)00072-7.

Gitelson, A.A., Gritz, Y., Merzlyak, M.N., 2003. Relationships between leaf chlorophyll content and spectral reflectance and algorithms for non-destructive chlorophyll assessment in higher plant leaves. J. Plant Physiol. 160, 271–282. https://doi.org/10.1078/0176-1617-00887.

Guyot, G., Baret, F., 1988. Utilisation de la haute resolution spectrale pour suivre l'etat des couverts vegetaux. Spectr. Signat. Objects Remote Sens. 287, 279.

Haboudane, D., Miller, J.R., Pattey, E., Zarco-Tejada, P.J., Strachan, I.B., 2004. Hyperspectral vegetation indices and novel algorithms for predicting green LAI of crop canopies: modeling and validation in the context of precision agriculture. Remote Sens. Environ. 90, 337–352. https://doi.org/10.1016/j.rse.2003.12.013.

Hensen, P.M., Schjoerring, J.K., 2003. Reflectance measurement of canopy biomass and nitrogen status in wheat crops using normalized difference vegetation indices and

partial least squares regression. Remote Sens. Environ. 86 (2003), 542–553.
Hernández-Clemente, R., Navarro-Cerrillo, R.M., Suárez, L., Morales, F., Zarco-Tejada, P.J., 2011. Assessing structural effects on PRI for stress detection in conifer forests. Remote Sens. Environ. 115, 2360–2375. https://doi.org/10.1016/j.rse.2011.04.036.
Heung, B., Bulmer, C.E., Schmidt, M.G., 2014. Predictive soil parent material mapping at a regional-scale: a random forest approach. Geoderma 214–215, 141–154. https://doi.org/10.1016/j.geoderma.2013.09.016.
Higgins, S., Schellberg, J., Bailey, J.S., 2017. A review of precision agriculture as an aid to nutrient management in intensive grassland areas in North West Europe. Adv. Anim. Biosci. 8 (2), 782–786. https://doi.org/10.1017/S2040470017000668.
Honkavaara, E., Khoramshahi, E., 2018. Radiometric correction of close-range spectral image blocks captured using an unmanned aerial vehicle with a radiometric block adjustment. Remote Sens. 10, 256. https://doi.org/10.3390/rs10020256.
Honkavaara, E., Saari, H., Kaivosoja, J., Pölönen, I., Hakala, T., Litkey, P., Mäkynen, J., Pesonen, L., 2013. Processing and assessment of spectrometric, stereoscopic imagery collected using a lightweight UAV spectral camera for precision agriculture. Remote Sens. 5, 5006–5039. https://doi.org/10.3390/rs5105006.
Honkavaara, E., Rosnell, T., Oliveira, R., Tommaselli, A., 2017. Band registration of tuneable frame format hyperspectral UAV imagers in complex scenes. ISPRS J. Photogramm. Remote Sens. 134, 96–109. https://doi.org/10.1016/j.isprsjprs.2017.10.014. 2017.
Hopkins, A., 2000. Herbage mass. In: Hopkins, Alan (Ed.), Grass: Its Production and Utilization, 3rd ed. Published for the British Grassland Society by Blackwell Science, pp. 90–110 Edited by.
Huhtanen, P., Nousiainen, J., Rinne, M., 2006. Recent developments in forage evaluation with special reference to practical applications. Agric. Food Sci. 15, 293–323.
Hyrkäs, M., Korhonen, P., Pitkänen, T., Rinne, M., Kaseva, J., 2016. Grass growth models for estimating digestibility and dry matter yield of forage grasses in Finland. Grassland Science in Europe 23, 252–254.
Knoblauch, C., Watson, C., Berendonk, C., Becker, R., Wrage-Mönnig, N., Wichern, F., 2017. Relationship between remote sensing data, plant biomass and soil nitrogen dynamics in intensively managed grasslands under controlled conditions. Sensors 17 (7), 1483.
Korhonen, P., Palosuo, T., Persson, T., Höglind, M., Jégo, G., Van Oijen, M., Gustavsson, A.-M., Bélanger, G., Virkajärvi, P., 2018. Modelling Grass Yields in Northern Climates – A Comparison of Three Growth Models for Timothy. 224. pp. 34–47. https://doi.org/10.1016/j.fcr.2018.04.014.
Kuoppala, K., 2010. Influence of harvesting strategy on nutrient supply and production of dairy cows consuming diets based on grass and red clover silage. Doctoral Dissertation In: MTT Science. 11 (99 p).
Li, W., Niu, Z., Chen, H., Li, D., Wu, M., Zhao, W., 2016. Remote estimation of canopy height and aboveground biomass of maize using high-resolution stereo images from a low-cost unmanned aerial vehicle system. Ecol. Indic. 67, 637–648. https://doi.org/10.1016/j.ecolind.2016.03.036.
Li, Z.W., Xin, X.P., Huan, T.A.N.G., Fan, Y.A.N.G., Chen, B.R., Zhang, B.H., 2017. Estimating grassland LAI using the Random Forests approach and Landsat imagery in the meadow steppe of Hulunber, China. J. Integr. Agric 16, 286–297. https://doi.org/10.1016/S2095-3119(15)61303-X.
Mäkynen, J., Holmlund, C., Saari, H., Ojala, K., Antila, T., 2011. Unmanned aerial vehicle (UAV) operated megapixel spectral camera. In: Electro-Optical Remote Sensing, Photonic Technologies, and Applications V. 8186. International Society for Optics and Photonics, Bellingham, WA, USA, pp. 81860Y 2011.
Meyer, G.E., Hindman, T.W., Laksmi, K., 1999. In: Meyer, G.E., DeShazer, J.A. (Eds.), Machine vision detection parameters for plant species identification. University of Nebraska, Lincoln, NE, USA, pp. 327–335.
Mulla, D.J., 2013. Twenty five years of remote sensing in precision agriculture: key advances and remaining knowledge gaps. Biosyst. Eng. 114, 358–371. https://doi.org/10.1016/j.biosystemseng.2012.08.009.
Näsi, R., Honkavaara, E., Lyytikäinen-Saarenmaa, P., Blomqvist, M., Litkey, P., Hakala, T., Viljanen, N., Kantola, T., Tanhuanpää, T., Holopainen, M., 2015. Using UAV-based photogrammetry and hyperspectral imaging for mapping bark beetle damage at tree-level. Remote Sens. 7 (11), 15467–15493. https://doi.org/10.3390/rs71115467.
Näsi, R., Viljanen, N., Kaivosoja, J., Alhonoja, K., Hakala, T., Markelin, L., Honkavaara, E., 2018. Estimating biomass and nitrogen amount of barley and grass using UAV and aircraft based spectral and photogrammetric 3D features. Remote Sens. 10 (7), 1082. https://doi.org/10.3390/rs10071082.
Neto, J.A, 2004. Combined Statistical-Soft Computing Approach for Classification and Mapping Weed Species in Minimum Tillage Systems. University of Nebraska, Lincoln, NE, USA, pp. 170.
Nevalainen, O., Honkavaara, E., Tuominen, S., Viljanen, N., Hakala, T., Yu, X., Hyyppä, J., Saari, H., Pölönen, I., Imai, N., 2017. Individual Tree Detection and Classification with UAV-Based Photogrammetric Point Clouds and Hyperspectral Imaging. Remote Sens 9, 185. https://doi.org/10.3390/rs9030185.
Nissinen, O., Kalliainen, P., Jauhiainen, L., 2010. Development of yield and nutritive value of timothy in primary growth and regrowth in northern growing conditions. Agric. Food Sci. 19, 252–268.
NLS, National Land Survey of Finland, 2018. Finnref GNSS RINEX Service. Available online. https://www.maanmittauslaitos.fi/en/maps-and-spatial-data/positioning-services/rinex-palvelu, Accessed date: 10 October 2018.
Norris, K.H., Barnes, R.F., Moore, J.E., Shenk, J.S., 1976. Predicting forage quality by infrared replectance spectroscopy 1. J. Anim. Sci. 43 (4), 889–897.
Oliveira, R.A., Tommaselli, A.M., Honkavaara, E., 2016. Geometric calibration of a hyperspectral frame camera. Photogramm. Rec. 31 (155), 325–347. https://doi.org/10.1111/phor.12153.
Oliveira, R.A., Tommaselli, A.M., Honkavaara, E., 2018. Generating a hyperspectral digital surface model using a hyperspectral 2D frame camera. ISPRS J. Photogramm. Remote Sens. 147, 345–360. https://doi.org/10.1016/j.isprsjprs.2018.11.025.
Pearson, R.L., Miller, L.D., 1972. Remote mapping of standing crop biomass for estimation of the productivity of the short-grass Prairie, Pawnee National Grasslands, Colorado. In Proceedings of the 8th International Symposium on Remote Sensing of Environment, Ann Arbor, MI, USA, pp. 1357–1381.
Persson, T., Höglind, M., Van Oijen, M., Korhonen, P., Palosuo, T., Jégo, G., Virkajärvi, P., Bélanger, G., Gustavsson, A.-M., 2019. Simulation of timothy nutritive value: a comparison of three process-based models. Fields Crops Research 231, 81–92. https://doi.org/10.1016/j.fcr.2018.11.008.
Pullanagari, R.R., Yule, I.J., Tuohy, M.P., Hedley, M.J., Dynes, R.A., King, W.M., 2012. In-field hyperspectral proximal sensing for estimating quality parameters of mixed pasture. Precis. Agric. 13 (3), 351–369. https://doi.org/10.1007/s11119-011-9251-4.
Pullanagari, R., Kereszturi, G., Yule, I., 2018. Integrating airborne hyperspectral, topographic, and soil data for estimating pasture quality using recursive feature elimination with random forest regression. Remote Sens. 10 (7), 1117. https://doi.org/10.3390/rs10071117.
Qi, J., Chehbouni, A., Huete, A.R., Kerr, Y.H., Sorooshian, S., 1994. A modified soil adjusted vegetation index. Remote Sens. Environ. 48, 119–126. https://doi.org/10.1016/0034-4257(94)90134-1.
Rinne, M., Jaakkola, S., Kaustell, K., Heikkilä, T., Huhtanen, P., 1999. Silages harvested at different stages of grass growth v. concentrate foods as energy and protein sources in milk production. Animal science 69, 251–263.
Rinne, M., 2000. Influence of the Timing of the Harvest or Primary Grass Growth on Herbage Quality and Subsequent Digestion and Performance in the Ruminant Animal. Academic dissertation. University of Helsinki. Dept. of Animal Science (Publications 54. 42 p).
Rondeaux, G., Steven, M., Baret, F., 1996. Optimization of soil-adjusted vegetation indices. Remote Sens. Environ. 55, 95–107. https://doi.org/10.1016/0034-4257(95)00186-7.
Roosjen, P.P.J., Brede, B., Suomalainen, J.M., Bartholomeus, H.M., Kooistra, L., Clevers, J.G.P.W., 2018. Improved estimation of leaf area index and leaf chlorophyll content of a potato crop using multi-angle spectral data – potential of unmanned aerial vehicle imagery. Int. J. Appl. Earth Obs. Geoinf. 66, 14–26. https://doi.org/10.1016/j.jag.2017.10.012.
Roujean, J.-L., n.d.Breon, F.-M. 1995 Estimating PAR absorbed by vegetation from bidirectional reflectance measurements. Remote Sens. Environ. 51, 375–384, doi:https://doi.org/10.1016/0034-4257(94)00114-3.
Rouse, J.W., 1974. Monitoring vegetation systems in the Great plains with ERTS. NASA, Washington, DC, USA, pp. 309–317.
RTKlib, 2018. RTKlib, an Open-source Program Package for GNSS Positioning, Version 2.4.2. Available online. www.rtklib.com, Accessed date: 10 November 2018.
Rymer, C., 2000. The measurement of forage digestibility in vivo. In: Givens, D.I., Owens, E., Axford, R.F.E., Omed, H.M. (Eds.), Forage Evaluation in Ruminant Nutrition. CABI, Wallingford, UK, pp. 113–134 (2000).
Sanderson, M.A., Rotz, C.A., Fultz, S.W., Rayburn, E.B., 2001. Estimating forage mass with a commercial capacitance meter, rising plate meter, and pasture ruler. Agron. J. 93, 1281–1286.
Schaepman-Strub, G., Schaepman, M.E., Painter, T.H., Dangel, S., Martonchik, J.V., 2006. Reflectance quantities in optical remote sensing – definitions and case studies. Remote Sens. Environ. 103 (1), 27–42. https://doi.org/10.1016/j.rse.2006.03.002.
Smith, G.M., Milton, E.J., 1999. The use of the empirical line method to calibrate remotely sensed data to reflectance. Int. J. Remote Sens. 20, 2653–2662. https://doi.org/10.1080/014311699211994.
Suomalainen, J., Hakala, T., de Oliveira, Alves, Markelin, L., Viljanen, N., Näsi, R., Honkavaara, E., 2018. A novel tilt correction technique for irradiance sensors and spectrometers on-board unmanned aerial vehicles. Remote Sensing 10 (12), 2068.
't Mannetje, L., 2000. Measuring biomass of grassland vegetation. In: Tmannetje, L., Jones, R.M. (Eds.), Field and Laboratory Methods for Grassland and Animal Production Research. CABI Publishing, pp. 151–177 Edited by.
Tilly, N., Aasen, H., Bareth, G., 2015. Fusion of plant height and vegetation indices for the estimation of barley biomass. Remote Sensing 7 (9), 11449–11480.
Tucker, C.J., 1979. Red and photographic infrared linear combinations for monitoring vegetation. Remote Sens. Environ. 8, 127–150. https://doi.org/10.1016/0034-4257(79)90013-0.
Viljanen, N., Honkavaara, E., Näsi, R., Hakala, T., Niemeläinen, O., Kaivosoja, J., 2018. A novel machine learning method for estimating biomass of grass swards using a photogrammetric canopy height model, images and vegetation indices captured by a drone. Agriculture 8 (5), 70. https://doi.org/10.3390/agriculture8050070.
Virkajärvi, P., 1999. Comparison of three indirect methods for prediction of herbage mass on timothy-meadow fescue pastures. Acta Agriculturae Scandinavica, Section B – Plant Soil Science 49 (2), 75–81. https://doi.org/10.1080/09064719950135579.
Virkajärvi, P., Hyrkäs, M., Pakarinen, K., Suomela, R., 2012. Importance of senescence and dead material on nutritive value of grass silage. In: Kuoppala, K., Rinne, M., Vanhatalo, A. (Eds.), Proceedings of the XVI international silage conference Hämeenlinna. MTT Agrifood Research Finland, University of Helsinki, Finland, pp. 188–189. http://urn.fi/URN:ISBN:978-952-487-385-7.
Woebbecke, D.M., Meyer, G.E., Von Bargen, K., Mortensen, D.A., 1995. Color indices for weed identification under various soil, residue, and lighting conditions. Trans. ASAE 38, 259–269. https://doi.org/10.13031/2013.27838.
Wu, C., 2013. Towards linear-time incremental structure from motion. In: International Conference on 3D Vision 3DV 2013, pp. 127–134. https://doi.org/10.1109/3DV.2013.25. Seattle, WA.
Yue, J., Yang, G., Li, C., Li, Z., Wang, Y., Feng, H., Xu, B., 2017. Estimation of winter wheat above-ground biomass using unmanned aerial vehicle-based snapshot hyperspectral sensor and crop height improved models. Remote Sens. 9, 708. https://doi.

org/10.3390/rs9070708.
Yue, J., Feng, H., Jin, X., Yuan, H., Li, Z., Zhou, C., Tian, Q., 2018. A comparison of crop parameters estimation using images from UAV-mounted snapshot hyperspectral sensor and high-definition digital camera. Remote Sens. 10 (7), 1138. https://doi.org/10.3390/rs10071138.
Zarco-Tejada, P.J., Guillén-Climent, M.L., Hernández-Clemente, R., Catalina, A., González, M.R., Martín, P., 2013. Estimating leaf carotenoid content in vineyards using high resolution hyperspectral imagery acquired from an unmanned aerial vehicle (UAV). Agric. For. Meteorol. 281–294, 171–l72. https://doi.org/10.1016/j.agrformet.2012.12.013.
Zeng, L., Chen, C., 2018. Using remote sensing to estimate forage biomass and nutrient contents at different growth stages. Biomass and bioenergy 115, 74–81. https://doi.org/10.1016/j.biombioe.2018.04.016.